ARTICLE

https://doi.org/10.1038/s41586-018-0027-0

Functional circuit architecture underlying parental behaviour

Johannes Kohl[1], Benedicte M. Babayan[2], Nimrod D. Rubinstein[1], Anita E. Autry[1], Brenda Marin-Rodriguez[1], Vikrant Kapoor[2], Kazunari Miyamishi[3], Larry S. Zweifel[4,5], Liqun Luo[3], Naoshige Uchida[2] & Catherine Dulac[1]*

Parenting is essential for the survival and wellbeing of mammalian offspring. However, we lack a circuit-level understanding of how distinct components of this behaviour are coordinated. Here we investigate how galanin-expressing neurons in the medial preoptic area (MPOA^{Gal}) of the hypothalamus coordinate motor, motivational, hormonal and social aspects of parenting in mice. These neurons integrate inputs from a large number of brain areas and the activation of these inputs depends on the animal's sex and reproductive state. Subsets of MPOA^{Gal} neurons form discrete pools that are defined by their projection sites. While the MPOA^{Gal} population is active during all episodes of parental behaviour, individual pools are tuned to characteristic aspects of parenting. Optogenetic manipulation of MPOA^{Gal} projections mirrors this specificity, affecting discrete parenting components. This functional organization, reminiscent of the control of motor sequences by pools of spinal cord neurons, provides a new model for how discrete elements of a social behaviour are generated at the circuit level.

Although essential for survival at a multigenerational time scale, parental care entails sacrifices without immediate benefits for the caregiver, suggesting that this behaviour is driven by evolutionarily shaped, hard-wired neural circuits[1,2]. Parenting, similar to other naturalistic behaviours, comprises multiple coordinated components, such as specific motor patterns, an enhanced motivation to interact with infants, distinct hormonal states and often the suppression of other social activities such as mating. We aimed to exploit the recent identification of MPOA^{Gal} neurons as a key node in the control of parenting in mice[3] to uncover organizational principles of associated neural circuits. We hypothesized that the function of MPOA^{Gal} neurons in parental behaviour requires integration of external signals, such as stimuli from pups and other environmental sources, and internal hormonal and metabolic information, as well as the ability to coordinate the motor, motivational, hormonal and social components of parenting.

Identity and activity of MPOA^{Gal} inputs

To determine brain-wide inputs into MPOA^{Gal} neurons, we used rabies virus-mediated retrograde trans-synaptic tracing[4] (Fig. 1a), and found that MPOA^{Gal} neurons receive direct inputs from more than 20 areas in both male and female mice (Fig. 1b, c, Extended Data Fig. 1a and Extended Data Table 1). Presynaptic neurons within the MPOA itself provided the highest fractional input (approximately 20%), and hypothalamic inputs accounted for about 60% of the presynaptic neurons, suggesting that extensive local processing occurs (Fig. 1c). MPOA^{Gal} neurons also receive inputs from monoaminergic and neuropeptidergic modulatory areas, the mesolimbic reward system, pathways associated with pheromone-processing, and hypothalamic as well as septal areas involved in emotional states (Fig. 1c and Extended Data Fig. 1a). Inputs from the paraventricular hypothalamic nucleus (PVN), a key area for homeostatic and neuroendocrine control, were particularly abundant. Notably, MPOA^{Gal} neurons did not receive direct inputs from oxytocin (OXT)-secreting PVN (PVN^{OXT}) neurons, which are implicated in parturition, lactation and maternal behaviour[1,2,5], but instead received inputs from vasopressin-expressing PVN (PVN^{AVP}) neurons, which are associated with the modulation of many social behaviours[6] and nest building[7] (Fig. 1d). MPOA^{Gal} neurons also received inputs from AVP^{+}, but not OXT^{+}, neurons of the supraoptic nucleus (Extended Data Fig. 1d). Input fractions were similar in males and females, with a few exceptions (Fig. 1e, f and Extended Data Fig. 1a). Therefore, MPOA^{Gal} neurons appear to be anatomically well-positioned to integrate external (sensory) as well as internal (modulatory) signals that are relevant to parenting in both sexes.

Next, we investigated MPOA^{Gal} input activation during parenting according to the animal's sex and reproductive state. In laboratory mice, virgin females and sexually experienced males and females show parental behaviours, whereas virgin males typically attack and kill pups[3,8,9]. We combined rabies tracing with immunostaining for the activity marker Fos after parenting in primiparous females (mothers), virgin females and fathers (Fig. 1g) and compared the Fos^{+} fraction of input neurons between parental animals and non-pup-exposed controls (Fig. 1h–j). Local MPOA inputs were specifically activated during parenting in all groups (Fig. 1h–j), whereas the activation of other inputs was dependent on sex and reproductive state: in parents, but not virgin females, a subset of reward-associated and modulatory inputs were activated (Fig. 1h–j). Presynaptic neurons in pheromone-processing pathways (the medial amygdala (MeA) and bed nucleus of the stria terminalis (BNST)) were selectively activated in fathers and virgin females, but not in mothers (Fig. 1h–j). Because pup-directed aggression in virgin mice is pheromone-dependent[3,8], the MeA–BNST pathway might remain partially active in sexually experienced males and parental virgin females, whereas it is fully silenced only in mothers. Intriguingly, the largest number of inputs was activated in fathers (Fig. 1j), and non-overlapping subsets of inputs were activated in mothers and virgin females (Fig. 1h, i). These results suggest that MPOA^{Gal} neurons perform different computations of inputs according to the animal's sex and reproductive state.

Input–output logic of the MPOA^{Gal} circuit

To identify MPOA^{Gal} projections and synaptic targets, we infected MPOA^{Gal} neurons with adeno-associated viruses (AAVs) encoding the fluorophore tdTomato as well as the presynaptic marker

[1]Howard Hughes Medical Institute, Department of Molecular and Cellular Biology, Center for Brain Science, Harvard University, Cambridge, MA, USA. [2]Department of Molecular and Cellular Biology, Center for Brain Science, Harvard University, Cambridge, MA, USA. [3]Howard Hughes Medical Institute, Department of Biology, Stanford University, Stanford, CA, USA. [4]Department of Pharmacology, University of Washington, Seattle, WA, USA. [5]Department of Psychiatry and Behavioral Sciences, University of Washington, Seattle, WA, USA. *e-mail: dulac@fas.harvard.edu

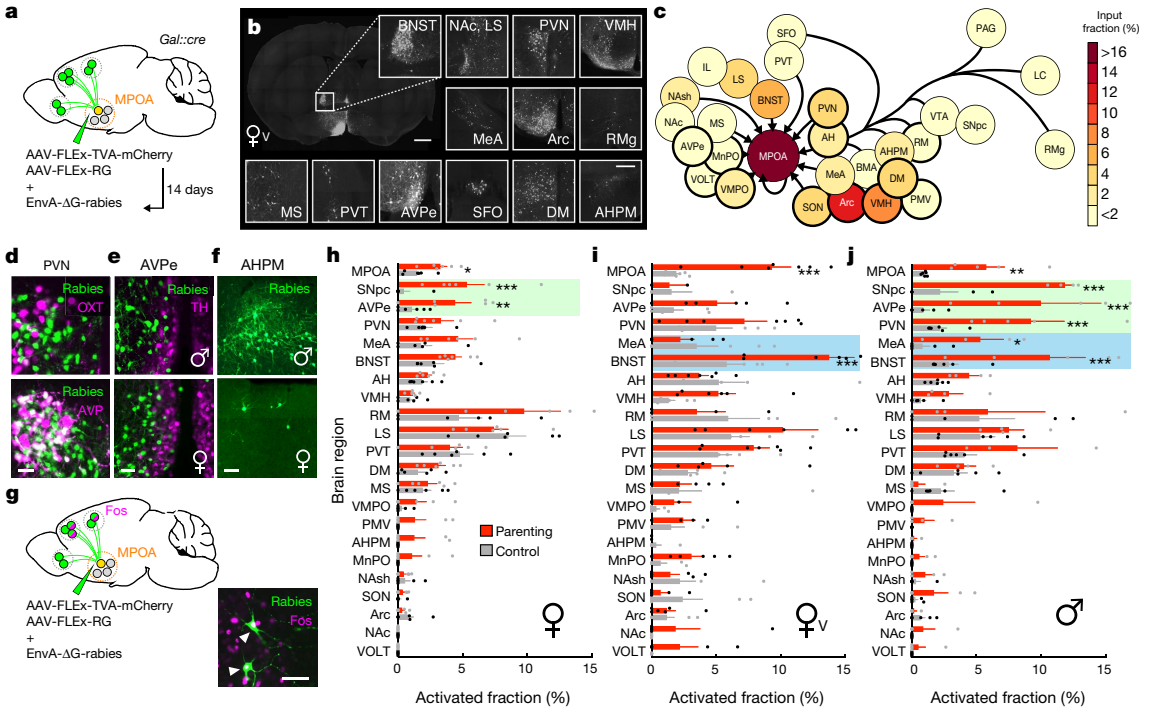

Fig. 1 | MPOA^{Gal} inputs are activated during parental behaviour in a sex- and reproductive state-specific manner. a, Monosynaptic retrograde tracing from MPOA^{Gal} neurons. **b**, Input areas with rabies^{+} neurons in a virgin female. **c**, Overview of inputs into MPOA^{Gal} neurons. Hypothalamic input areas are circled in bold. **d**, MPOA^{Gal} neurons receive monosynaptic inputs from magnocellular PVN^{AVP} (37.6 ± 4.1% overlap, $n = 3$ mice) but rarely from PVN^{OXT} (2.6 ± 0.6%, $n = 3$ mice) neurons. **e**, Presynaptic neurons in AVPe are TH^{-} in males (1.9% TH^{+}, $n = 2$ mice) and females (1.8% TH^{+}, $n = 3$ mice). **f**, Presynaptic neurons in posteriomedial amygdalo-hippocampal area (AHPM). **g**, Identification of activated MPOA^{Gal} inputs and example of Fos^{+} presynaptic neurons. **h**–**j**, Activated input fractions in mothers (**h**), virgin females (**i**) and fathers (**j**). $n = 6$ pup-exposed mice, $n = 6$ controls each. Green boxes, parent-specific activation; blue boxes, father- and virgin female-specific activation. Two-tailed t-tests (corrected for multiple comparisons, Methods); **h**, $^{***}P < 0.0001$, $^{**}P = 0.0267$, $^{*}P = 0.0196$; **i**, $^{***}P < 0.0001$; **j**, $^{***}P < 0.0001$, $^{**}P = 0.0035$, $^{*}P = 0.0104$. **h**–**j**, Data are mean ± s.e.m.; n = number of mice in all figures. Scale bars, 500 μm (**b**, left), 250 μm (**b**, inset) and 50 μm (**d**–**g**). For definitions of the abbreviations, see Extended Data Table 1.

synaptophysin conjugated to GFP (Syn–GFP; Fig. 2a and Extended Data Fig. 2a). MPOA^{Gal} neurons project to approximately 20 areas in males and females (Fig. 2b, c and Extended Data Fig. 2b). Many of these regions were previously shown to be involved in maternal behaviour using pharmacological manipulations and lesions, mainly in rats[10] (Extended Data Table 2). Notably, this projection map mostly overlaps with the input map defined above (Fig. 1c), revealing extensive reciprocal connectivity in parental circuits.

Among the areas most intensely labelled by Syn–GFP were the PVN and anteroventral periventricular nucleus (AVPe) (Fig. 2c), which have both been implicated in the control of parenting[6,11]. Using rabies tracing from molecularly defined PVN cell types (Fig. 2d), we found that MPOA^{Gal} neurons project to PVN^{AVP}, PVN^{OXT} and corticotropin-releasing hormone (CRH)-expressing PVN neurons (PVN^{CRH}) in both males and females (Fig. 2e–g). Furthermore, connectivity from MPOA^{Gal} neurons to PVN neurons appears sexually dimorphic, with more MPOA^{Gal} neurons projecting to PVN^{AVP} and PVN^{CRH} neurons in males and more MPOA^{Gal} neurons projecting to PVN^{OXT} neurons in females (Fig. 2e–g). MPOA^{Gal} neurons might therefore exert control over parenting-promoting hormonal release in a sex-specific fashion.

Tyrosine-hydroxylase (TH)-expressing neurons in the AVPe were found to influence parenting in females via monosynaptic connections[11] from AVPeTH to PVN^{OXT} neurons. Rabies tracing from MPOA^{Gal} or AVPeTH neurons showed that whereas MPOA^{Gal} neurons do not receive monosynaptic inputs from AVPeTH neurons (Fig. 1e), AVPeTH neurons do receive direct inputs from MPOA^{Gal} neurons in both males and females (Extended Data Fig. 2e, f). Thus, MPOA^{Gal} neurons might also influence OXT secretion via a disynaptic circuit from MPOA^{Gal}→AVPeTH→PVN^{OXT} neurons (Extended Data Fig. 2g).

We next investigated the organization of MPOA^{Gal} projections, and their activity during parenting. Injections of the retrograde tracer cholera toxin subunit B (CTB) into pairs of MPOA^{Gal} projection targets revealed few double-labelled MPOA^{Gal} neurons (Extended Data Fig. 3a–c). Moreover, retrogradely labelled cell bodies from individual projections occupied characteristic, mostly non-overlapping zones in the MPOA (Extended Data Fig. 3f, g) and conditional tracing of individual projection areas identified only minor collaterals (Extended Data Fig. 4). These results suggest that MPOA^{Gal} neurons are organized in distinct pools, each projecting to mostly non-overlapping target areas. To assess whether different MPOA^{Gal} pools, as defined by their projection sites, were equally activated during parenting, we used a Cre-dependent, retrograde canine adenovirus (CAV) to label MPOA^{Gal} subpopulations projecting to regions that have previously been implicated in parenting (12 out of 22 projections; Extended Data Table 2) and quantified their activation in parental females (Fig. 2h). Fractions of Fos^{+} neurons differed widely between projections, ranging from more than 50% (projections to the periaqueductal grey (PAG)) to less than 10% (projections to the ventromedial hypothalamus, Fig. 2i). A similar distribution was found in parental fathers (Extended Data Fig. 2d).

On the basis of their high projection density (Fig. 2c), high activity during parenting (Fig. 2i) and potentially diverse contributions to this behaviour (Extended Data Table 2), we selected MPOA^{Gal} subpopulations that projected to the PAG, MeA, ventral tegmental area (VTA) and PVN for further characterization. Gal^{+} neurons were approximately twice more likely to project to most of these candidate areas than expected from their frequency in the MPOA (Extended Data Fig. 3d, e), supporting the hypothesis that these projections have prominent roles in the control of parenting.

We next aimed to determine whether projection-defined MPOA^{Gal} subpopulations receive selected inputs from the approximately 20 identified upstream areas (Fig. 1c) or whether they uniformly integrate all inputs. We used a double-conditional approach in which rabies virus

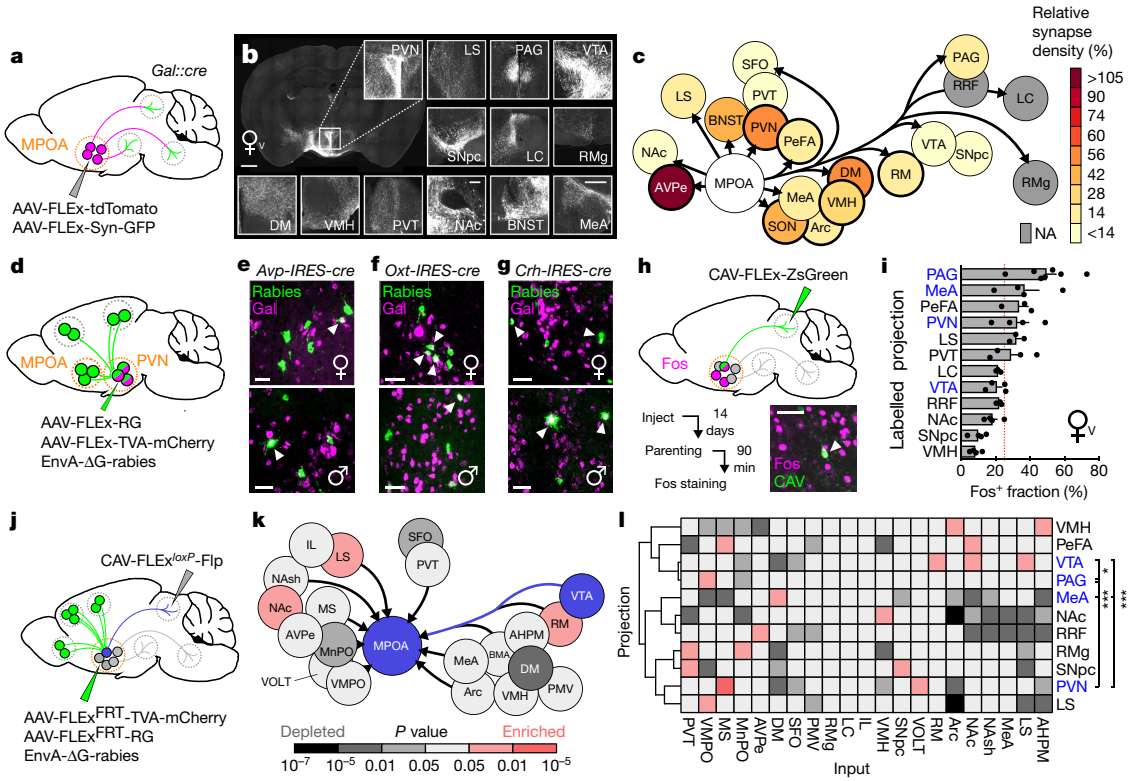

Fig. 2 | Identification of parenting-activated MPOA^{Gal} projections and input–output logic of the MPOA^{Gal} circuit. a, Visualization of MPOA^{Gal} projections. **b**, MPOA^{Gal} projections identified by tdTomato fluorescence in virgin females. **c**, Relative synaptic density in MPOA^{Gal} projection targets ($n = 4$ mice, Methods). Grey regions could not be quantified owing to tissue autofluorescence. Hypothalamic target areas are circled in bold. **d**, Monosynaptic retrograde tracing from PVN. **e**–**g**, MPOA^{Gal} neurons are presynaptic to PVN^{AVP} (**e**; female: 15 out of 364 Gal$^+$ neurons, $n = 3$; male: 46 out of 180 Gal$^+$ neurons, $n = 3$), to PVN^{OXT} (**f**; female: 26 out of 71 Gal$^+$ neurons, $n = 3$; male: 7 out of 51 Gal$^+$ neurons, $n = 3$) and to PVN^{CRH} neurons (**g**; female: 19 out of 72 Gal$^+$ neurons, $n = 3$; male: 22 out of 45 Gal$^+$ neurons, $n = 3$). Significantly more MPOA neurons presynaptic to PVN^{AVP} and PVN^{CRH} neurons were Gal$^+$ in males than in females ($P < 0.0001$ and $P = 0.0170$, respectively, two-tailed Fisher's exact test), whereas more MPOA neurons presynaptic to PVN^{OXT} neurons were Gal$^+$ in females than in males ($P = 0.0068$). **h**, Labelling strategy for MPOA^{Gal} projections; example of retrogradely labelled Fos$^+$ neuron in the MPOA. **i**, Activated fraction of MPOA^{Gal} neurons projecting to parenting-relevant brain areas ($n = 7, 4, 3, 4, 3, 4, 3, 4, 3, 4, 4, 4$ mice, from top to bottom). Data are mean ± s.e.m. Red line, population average[3]. Projections chosen for further functional studies are labelled in blue. **j**, Strategy for monosynaptic retrograde tracing from projection-defined MPOA^{Gal} subpopulations. **k**, **l**, Map of monosynaptic inputs into VTA-projecting MPOA^{Gal} neurons (**k**) and matrix displaying inputs into projection-defined MPOA^{Gal} subpopulations (**l**; see Methods; $n = 5, 3, 4, 4, 4, 4, 5, 5, 4, 4, 3$ mice, from top to bottom). A Tukey post hoc test was used to assess whether candidate projections (blue) receive quantitatively different inputs. VTA versus PAG, $^*P = 0.0205$; PAG versus PVN, $^{***}P = 0.0002$; all other comparisons, $^{***}P < 0.0001$. Scale bars, 500 μm (**b**, left) 250 μm (**b**, inset) and 50 μm (**e**–**g**, **h**).

can only infect neurons that project to an area of choice[12] (Fig. 2j and Extended Data Fig. 5b–d). We found that MPOA^{Gal} projections integrate broad input combinations, with characteristic sets of enriched or depleted inputs (Fig. 2k, l). This is seen for projections from the PAG, MeA, PVN and VTA, which receive similar, albeit quantitatively different, inputs (Fig. 2l). Notably, inputs from the nucleus accumbens and lateral septum, areas involved in reward and emotional responses, respectively, were specifically enriched in VTA-projecting MPOA^{Gal} neurons (Fig. 2k, l). Together, these findings suggest a circuit architecture in which broad input combinations converge onto largely non-overlapping, projection-defined MPOA^{Gal} subpopulations. These subpopulations may in turn be differentially activated during parenting by integrating across quantitatively different sets of activated inputs.

Specific activity of MPOA^{Gal} pools

We next used fibre photometry[13,14] (Fig. 3a, b) to investigate whether individual MPOA^{Gal} subpopulations are active during specific parenting steps. Conditional expression of the calcium reporter GCaMP6m in MPOA^{Gal} neurons was achieved by viral injection (Extended Data Fig. 6a) and an optical fibre was implanted above the injection site (Extended Data Fig. 6b–d). The entire (pan-MPOA^{Gal}) population displayed high activity during all pup-directed parenting episodes in mothers, virgin females and fathers (Fig. 3c–g and Supplementary Video 1), but not during non-pup-directed (nest building) or passive (crouching) parenting episodes (Fig. 3h, i). MPOA^{Gal} activation was stimulus-specific: interactions with adults resulted in minimal activity (Extended Data Fig. 6k, l). Moreover, orofacial motor actions similar to pup interactions did not activate MPOA^{Gal} neurons, confirming that the observed signals were not motion-related. The tuning of MPOA^{Gal} neurons during parenting was similar in all three groups (Fig. 3q)—highlighting their common role in the control of parental interactions. Activation during pup sniffing was higher in mothers than in virgin females and fathers (Fig. 3c), possibly reflecting the very high sensitivity of postpartum females to pup stimuli[15] (Extended Data Fig. 7). Furthermore, activity decreased in mothers—but not in fathers—during eating, self-grooming and sniffing of food (Fig. 3j–l). MPOA^{Gal} neurons receive their second-largest fractional input from the arcuate nucleus, a feeding control centre[16] (Fig. 1c and Extended Data Fig. 1a), suggesting that inhibition from circuits controlling mutually exclusive motor patterns, such as eating and pup grooming, might cause this decrease in activity.

To record the activity of projection-defined MPOA^{Gal} subpopulations, we injected MPOA^{Gal} target areas with a Cre-dependent, GCaMP6-expressing herpes simplex virus and implanted an optical fibre above the retrogradely labelled cell bodies (Fig. 3m and Extended Data Fig. 6e–h). PAG-projecting MPOA^{Gal} neurons were specifically activated during pup grooming (Fig. 3n and Extended Data Fig. 6m–q), whereas MeA-projecting MPOA^{Gal} neurons were active during most

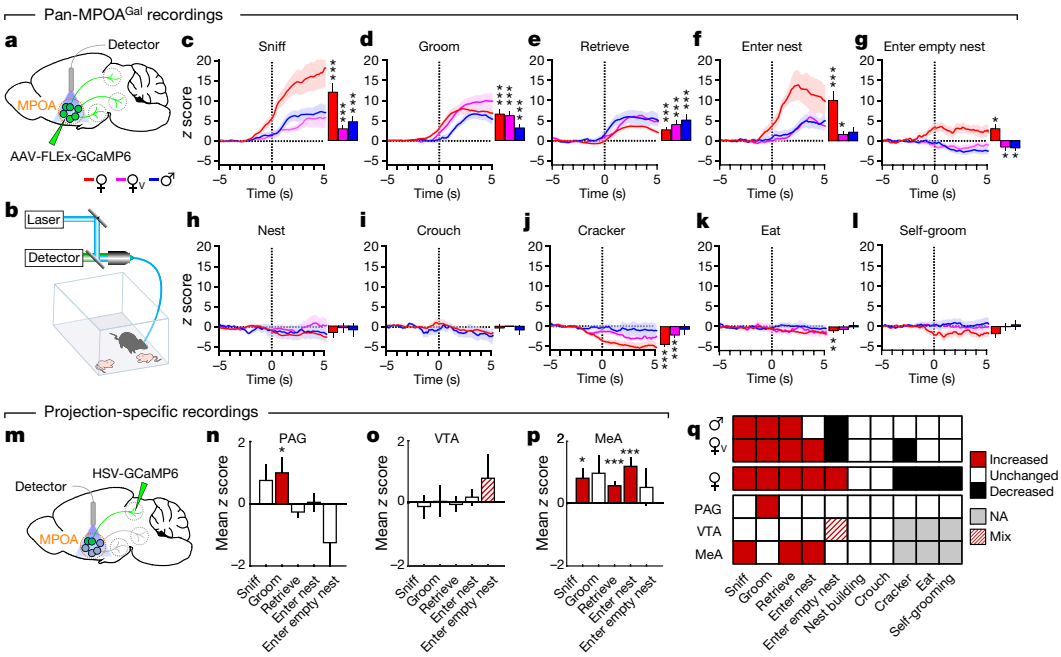

Fig. 3 | Distinct projection-defined MPOA^{Gal} neuronal pools are tuned to specific aspects of parental behaviour. a, **b**, Fibre photometry recording strategy (**a**) and setup (**b**). **c**–**i**, Averaged recording traces from MPOA^{Gal} population activity during pup sniffing (**c**), pup grooming (**d**), pup retrieval (**e**), entering a nest with pups (**f**), entering an empty nest (**g**), nest building (**h**) and crouching (**i**). Red, mother; pink, virgin female; blue, male. Mean peak activity (*z* scores) shown in mothers ($n = 4$), virgin females ($n = 3$) and fathers ($n = 5$). **j**–**l**, Averaged recording traces and mean peak activity during control behaviours. Cracker indicates sniffing of a pup-sized food object. **m**, Strategy for recording projection-defined MPOA^{Gal} subpopulations. **n**–**p**, Mean peak activation for MPOA^{Gal} neurons projecting to PAG (**n**, $n = 10$ mice), VTA (**o**, $n = 12$ mice) and MeA (**p**, $n = 8$ mice) during parenting. **q**, Tuning matrix for pan-MPOA^{Gal} (top) and projection-specific (bottom) recordings. Red, increased; white, unchanged; black, decreased; NA, not available (grey). Two-tailed *t*-tests (Methods). **c**, $^{***}P < 0.0001$, $^{***}P < 0.0001$, $^{***}P = 0.0001$ (from left to right); **d**, $^{***}P < 0.0001$; **e**, $^{***}P < 0.0001$, $^{***}P = 0.0008$, $^{***}P = 0.0004$ (from left to right); **f**, $^{***}P < 0.0001$, $^{*}P = 0.0247$; **g**, $^{*}P = 0.0185$, $^{*}P = 0.0365$, $^{*}P = 0.0105$ (from left to right); **j**, $^{***}P = 0.0002$, $^{***}P < 0.0001$ (from left to right); **k**, $^{**}P = 0.0059$; **n**, $^{*}P = 0.0362$; **p**, $^{*}P = 0.0102$, $^{***}P < 0.0001$, $^{***}P = 0.0001$ (from left to right). Data are mean ± s.e.m.

episodes of parental behaviour (Fig. 3p and Extended Data Fig. 6m–q), indicating a more general role in parenting. Consistent with their weak Fos activation after parenting (Fig. 2i), no significant activity changes were detected in VTA-projecting MPOA^{Gal} neurons (Fig. 3o and Extended Data Fig. 6m–p). Nevertheless, MPOA^{Gal} neurons signalling to VTA neurons were weakly responsive during nest entering in a subset of animals (Fig. 3o and Extended Data Fig. 6q; 4 out of 12 mice), potentially reflecting the expectation or drive to interact with pups. Taken together, these findings support the idea that MPOA^{Gal} neurons form functionally distinct modules that are tuned to specific parenting episodes.

Functionally distinct MPOA^{Gal} pools

We tested the hypothesis that MPOA^{Gal} neurons form functionally specialized pools by optogenetically activating projections to PAG, VTA and MeA during pup interactions (Fig. 4a). We virally expressed channelrhodopsin-2 (ChR2) in MPOA^{Gal} neurons (Extended Data Fig. 8a), and implanted optical fibres above MPOA^{Gal} projection targets. Optogenetic activation of MPOA^{Gal} to PAG projections at axon terminals did not affect the fraction of parental virgin females but suppressed pup attacks in infanticidal virgin males (Fig. 4b), and—consistent with MPOA^{Gal} to PAG activity during parenting (Fig. 3n)—increased pup grooming and pup-directed sniffing bouts in both males and females (Fig. 4c and Extended Data Fig. 8c). Next, we assessed the motivation to interact with pups by inserting a climbable barrier in the home cage between the test animal and pups (Fig. 4d). Activation of MPOA^{Gal} to PAG projections had no effect on the number of barrier crosses (Fig. 4d). Importantly, the effects of activation of MPOA^{Gal} to PAG projections were specific to pup interactions, and did not affect interactions with adult conspecifics (Fig. 4e, f).

By contrast, activation of MPOA^{Gal} to VTA projections did not affect pup interactions (Fig. 4g, h), but increased barrier crossing in both males and females (Fig. 4i and Supplementary Video 2), indicating an increased motivation to interact with pups. Interestingly, virgin males still exhibited pup-directed aggression after crossing the barrier, suggesting that this effect is not contingent upon the display of parenting. Nevertheless, in naturalistic situations, MPOA^{Gal} neurons and associated VTA projections are activated exclusively during parental interactions, thus specifically mediating parental drive. MPOA^{Gal} to VTA activation did not increase locomotion (Extended Data Fig. 8j, k) and did not affect interactions with intruders of either sex (Fig. 4j, k).

Finally, activation of MPOA^{Gal} to MeA projections did not affect pup-directed behaviours (Fig. 4l, m and Extended Data Fig. 7f, g)—except for a decrease in the amount of time spent in the nest in the females (Extended Data Fig. 8f)—or the motivation to interact with pups (Fig. 4n). However, this manipulation significantly inhibited male–male aggression and chemoinvestigation of a male intruder in females (Fig. 4o, p). Thus, instead of directly influencing parental behaviour, MPOA^{Gal} to MeA activation inhibits social interactions with adult conspecifics.

We tested the necessity of these subpopulations for discrete behaviours by expressing the inhibitory opsin eNpHR3.0 in MPOA^{Gal} neurons and stimulating their projections in virgin females (Fig. 4q, t, w). Consistent with ChR2 data, optogenetic inhibition of MPOA^{Gal} to PAG projections significantly reduced pup grooming and pup-directed sniffing bouts (Fig. 4s and Extended Data Fig. 8n), without affecting other behaviours (Fig. 4r and Extended Data Fig. 8n–p, u). By contrast, inhibition of MPOA^{Gal} to VTA projections specifically reduced barrier crossing frequency (Fig. 4v, u and Extended Data Fig. 8q, r, v), except for a reduction in time spent in the nest (Extended Data Fig. 8q). Finally, inhibition of MPOA^{Gal} to MeA projections did not affect interactions with an intruder (Fig. 4y) or other behaviours (Fig. 4x and Extended Data Fig. 8s, t, w). Recent findings indicate that representations of social stimuli in MeA and hypothalamic centres

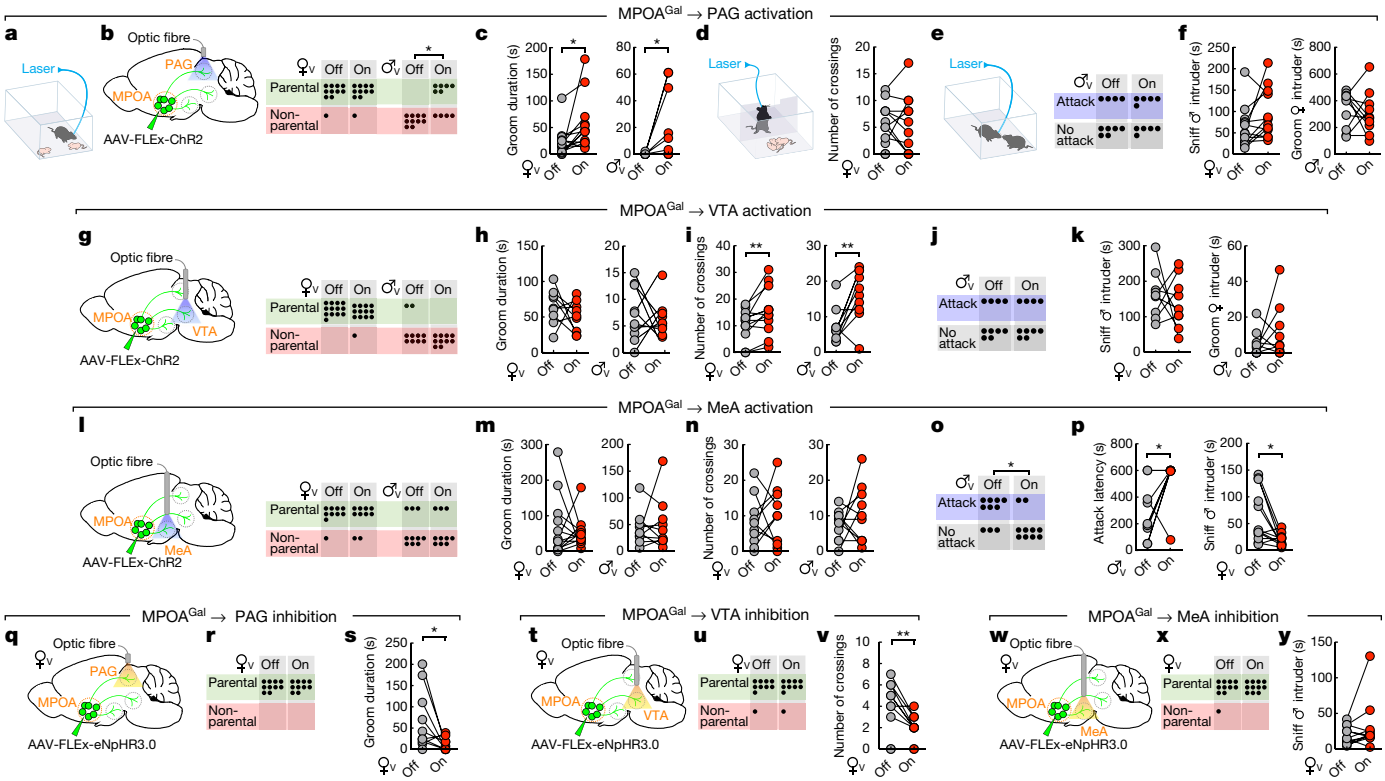

Fig. 4 | MPOA^{Gal} projections mediate discrete aspects of parental behaviour. a, Setup for optogenetic manipulations. **b**, **g**, **l**, Left, activation of MPOA^{Gal} projections. Right, pup-directed behaviour in virgin females and males without (Off) or with (On) activation of MPOA^{Gal} to PAG (**b**), VTA (**g**) and MeA (**l**) projections. Dots indicate the number of animals. **c**, **h**, **m**, Effect of activating MPOA^{Gal} to PAG (**c**; $n = 13$ virgin females; $n = 9$ virgin males), VTA (**h**; $n = 9$ virgin females; $n = 10$ virgin males) or MeA (**m**; $n = 10$ virgin females; $n = 10$ virgin males) projections on pup grooming. **d**, Motivation assay. **d**, **i**, **n**, Effect of activating MPOA^{Gal} to PAG (**d**; $n = 13$ virgin females), VTA (**i**; $n = 10$ virgin females; $n = 13$ virgin males) or MeA (**n**; $n = 10$ virgin females; $n = 10$ virgin males) projections on barrier crossing. **e**, Intruder assay. **e**, **j**, **o**, Effect of activating MPOA^{Gal} to PAG (**e**; $n = 10$ virgin males), VTA (**j**; $n = 10$ virgin males) or MeA (**o**; $n = 10$ virgin males) projections on male–male aggression. **f**, **k**, Effect of activating PAG (**f**) or VTA (**k**) projections on male- ($n = 12$ virgin females (**f**), $n = 9$ virgin females (**k**)) or female-directed ($n = 10$ virgin males (**f**), $n = 10$ virgin males (**k**)) behaviour. **p**, Effect of activating MPOA^{Gal} to MeA projections on male-directed attack latency ($n = 10$ virgin males) and chemoinvestigation ($n = 10$ virgin females). **q**, **t**, **w**, Inhibition of MPOA^{Gal} projections. **r**, **u**, **x**, Pup-directed behaviour in virgin females without (Off) or with (On) inhibition of PAG (**r**; $n = 10$), VTA (**u**; $n = 10$) and MeA (**x**; $n = 11$) projections. **s**, Effect of inhibiting MPOA^{Gal} to PAG projections on pup grooming ($n = 10$). **v**, Effect of inhibiting MPOA^{Gal} to VTA projections on barrier crossing ($n = 10$). **y**, Effect of inhibiting MPOA^{Gal} to MeA projections on male-directed chemoinvestigation ($n = 11$). χ^2 tests (**b**, **e**, **g**, **j**, **l**, **o**, **r**, **u**, **x**) or two-tailed paired *t*-tests (**c**, **d**, **f**, **h**, **i**, **k**, **m**, **n**, **p**, **s**, **v**, **y**) were used. **b**, $^{**}P = 0.0034$; **c**, $^{*}P = 0.0273$, $^{*}P = 0.0374$; **i**, $^{**}P = 0.0089$, $^{**}P = 0.0056$; **o**, $^{*}P = 0.0246$; **p**, $^{*}P = 0.033$, $^{*}P = 0.0109$; **s**, $^{*}P = 0.0396$; **v**, $^{**}P = 0.0038$.

change significantly after sexual experience[17,18]. Thus, low basal activity in this circuit branch in virgin females compared to mothers may preclude further inhibition. Alternatively, or additionally, this lack of effect may result from a more complex role of the connectivity from MPOA^{Gal} neurons projecting to MeA.

Concluding remarks

Taken together, our data suggest that distinct MPOA^{Gal} pools control discrete aspects of parental behaviour in both sexes (Fig. 5). Consistent with a role of the PAG in motor aspects of maternal behaviour[2], MPOA^{Gal} to PAG projections promote pup grooming. Retrograde tracing from PAG showed that MPOA^{Gal} neurons synapse with GABAergic (γ-aminobutyric-acid-releasing, inhibitory), but not glutamatergic (excitatory) PAG neurons (Extended Data Fig. 2h–j). Because the vast majority (around 90%) of MPOA^{Gal} neurons are GABAergic[3], pup grooming is probably elicited by disinhibition in the PAG. Indeed, infusion of the PAG with the $GABA_A$ receptor antagonist bicuculline increases pup licking and grooming[19]. By contrast, MPOA^{Gal} to VTA projections specifically influence the motivation to interact with pups without affecting the quality of adult–infant interactions. This is consistent with the proposed role of the VTA in motivation[20] and social reinforcement[21], and complements previous findings in rats[2,22]. Nearby Gal$^+$ neurons in the lateral hypothalamus promote food-seeking behaviour, despite lacking VTA projections[23], further highlighting the specific role of MPOA^{Gal} neurons in parenting. Finally, we found that MPOA^{Gal} to MeA projections do not directly influence pup-directed behaviour, but instead inhibit potentially competing adult social interactions.

Interestingly, MPOA^{Gal} to MeA projections are active during most episodes of parenting (Fig. 3p, q), suggesting that the entire behaviour, rather than specific parenting components, are broadcast by this projection to influence the vomeronasal pathway[24–26]. Specific inhibitory feedback from MPOA^{Gal} to MeA projections might impair the detection, or alter the valence, of non-pup-related social stimuli. Indeed, optogenetic stimulation of glutamatergic neurons in the posteriodorsal MeA—the MeA compartment that is most densely innervated by MPOA^{Gal} fibres (Fig. 2b)—has been shown to suppress interactions with adult conspecifics[27]. The projections investigated here mediate crucial, non-overlapping aspects of parental behaviour and the sum of their activity profiles matches that of the entire MPOA^{Gal} population (Fig. 3q). Thus, combined with the finding that MPOA^{Gal} neurons contact AVP-, OXT- and CRH-expressing PVN neurons (Fig. 2e–g), we have dissected circuit branches for four major—motor, motivational, social and neuromodulatory—aspects of parenting control. Other MPOA^{Gal} projections that have not been included here may have additional roles in parenting. Lastly, our tracing data suggest extensive connectivity within the MPOA (Fig. 1c), hinting at interactions between functionally specialized MPOA^{Gal} subpopulations.

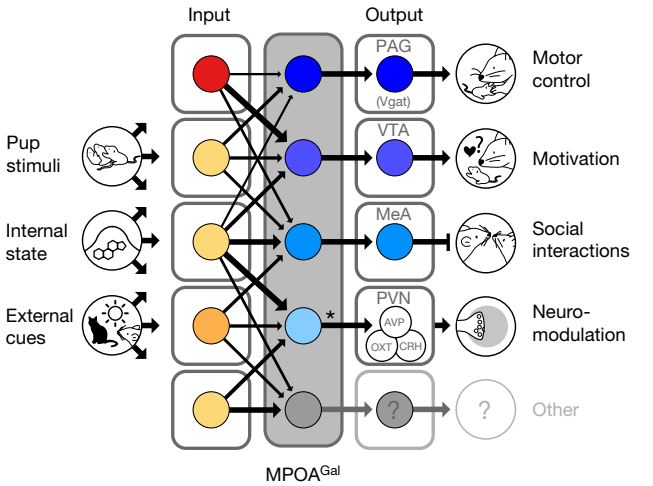

Fig. 5 | Functional architecture of the MPOA^{Gal} circuit. Broad, state- and sex-specifically activated inputs converge onto largely non-overlapping, projection-defined MPOA^{Gal} subpopulations that elicit specific aspects of parental behaviour. *MPOA^{Gal} to PVN connections are sexually dimorphic (see Fig. 2e–g).

Considerable progress has recently been made in identifying neuronal populations that control specific social behaviours or homeostatic functions[10,16,28–31]. However, little is known about how these multi-component behaviours or functions are orchestrated at the circuit level. Intriguingly, the modular architecture uncovered here for the control of parenting is reminiscent of the motor circuit motif that has been identified in the mammalian spinal cord, in which discrete phases of locomotor sequences are controlled by functionally distinct neuronal pools with highly specific connectivity patterns[32]. Whether other social behaviours rely on similar circuit architectures remains to be determined.

Online content

Any Methods, including any statements of data availability and Nature Research reporting summaries, along with any additional references and Source Data files, are available in the online version of the paper at https://doi.org/10.1038/s41586-018-0027-0.

Received: 4 August 2017; Accepted: 13 February 2018;
Published online: 11 April 2018

1. Dulac, C., O'Connell, L. A. & Wu, Z. Neural control of maternal and paternal behaviors. *Science* **345**, 765–770 (2014).
2. Numan, M. & Insel, T. R. *The Neurobiology of Parental Behavior* (Springer, New York, 2011).
3. Wu, Z., Autry, A. E., Bergan, J. F., Watabe-Uchida, M. & Dulac, C. G. Galanin neurons in the medial preoptic area govern parental behaviour. *Nature* **509**, 325–330 (2014).
4. Wickersham, I. R. et al. Monosynaptic restriction of transsynaptic tracing from single, genetically targeted neurons. *Neuron* **53**, 639–647 (2007).
5. Marlin, B. J., Mitre, M., D'Amour, J. A., Chao, M. V. & Froemke, R. C. Oxytocin enables maternal behaviour by balancing cortical inhibition. *Nature* **520**, 499–504 (2015).
6. Johnson, Z. V. & Young, L. J. Oxytocin and vasopressin neural networks: Implications for social behavioral diversity and translational neuroscience. *Neurosci. Biobehav. Rev.* **76**, 87–98 (2017).
7. Bendesky, A. et al. The genetic basis of parental care evolution in monogamous mice. *Nature* **544**, 434–439 (2017).
8. Tachikawa, K. S., Yoshihara, Y. & Kuroda, K. O. Behavioral transition from attack to parenting in male mice: a crucial role of the vomeronasal system. *J. Neurosci.* **33**, 5120–5126 (2013).
9. Vom Saal, F. S. Time-contingent change in infanticide and parental behavior induced by ejaculation in male mice. *Physiol. Behav.* **34**, 7–15 (1985).
10. Kohl, J., Autry, A. E. & Dulac, C. The neurobiology of parenting: a neural circuit perspective. *BioEssays* **39**, 1–11 (2017).
11. Scott, N., Prigge, M., Yizhar, O. & Kimchi, T. A sexually dimorphic hypothalamic circuit controls maternal care and oxytocin secretion. *Nature* **525**, 519–522 (2015).
12. Schwarz, L. A. et al. Viral-genetic tracing of the input–output organization of a central noradrenaline circuit. *Nature* **524**, 88–92 (2015).
13. Gunaydin, L. A. et al. Natural neural projection dynamics underlying social behavior. *Cell* **157**, 1535–1551 (2014).
14. Kudo, Y. et al. A single optical fiber fluorometric device for measurement of intracellular $Ca2^{+}$ concentration: its application to hippocampal neurons *in vitro* and *in vivo*. *Neuroscience* **50**, 619–625 (1992).
15. Elyada, Y. M. & Mizrahi, A. Becoming a mother—circuit plasticity underlying maternal behavior. *Curr. Opin. Neurobiol.* **35**, 49–56 (2015).
16. Andermann, M. L. & Lowell, B. B. Toward a wiring diagram understanding of appetite control. *Neuron* **95**, 757–778 (2017).
17. Li, Y. et al. Neuronal representation of social information in the medial amygdala of awake behaving mice. *Cell* **171**, 1176–1190 (2017).
18. Remedios, R. et al. Social behaviour shapes hypothalamic neural ensemble representations of conspecific sex. *Nature* **550**, 388–392 (2017).
19. Lee, G. & Gammie, S. C. $GABA_A$ receptor signaling in caudal periaqueductal gray regulates maternal aggression and maternal care in mice. *Behav. Brain Res.* **213**, 230–237 (2010).
20. Salamone, J. D. & Correa, M. The mysterious motivational functions of mesolimbic dopamine. *Neuron* **76**, 470–485 (2012).
21. McHenry, J. A. et al. Hormonal gain control of a medial preoptic area social reward circuit. *Nat. Neurosci.* **20**, 449–458 (2017).
22. Seip, K. M. & Morrell, J. I. Transient inactivation of the ventral tegmental area selectively disrupts the expression of conditioned place preference for pup- but not cocaine-paired contexts. *Behav. Neurosci.* **123**, 1325–1338 (2009).
23. Qualls-Creekmore, E. et al. Galanin-expressing GABA neurons in the lateral hypothalamus modulate food reward and noncompulsive locomotion. *J. Neurosci.* **37**, 6053–6065 (2017).
24. Isogai, Y. et al. Molecular organization of vomeronasal chemoreception. *Nature* **478**, 241–245 (2011).
25. Bergan, J. F., Ben-Shaul, Y. & Dulac, C. Sex-specific processing of social cues in the medial amygdala. *eLife* **3**, e02743 (2014).
26. Yao, S., Bergan, J., Lanjuin, A. & Dulac, C. Oxytocin signaling in the medial amygdala is required for sex discrimination of social cues. *eLife* **6**, e31373 (2017).
27. Hong, W., Kim, D. W. & Anderson, D. J. Antagonistic control of social versus repetitive self-grooming behaviors by separable amygdala neuronal subsets. *Cell* **158**, 1348–1361 (2014).
28. Anderson, D. J. Circuit modules linking internal states and social behaviour in flies and mice. *Nat. Rev. Neurosci.* **17**, 692–704 (2016).
29. Yang, T. & Shah, N. M. Molecular and neural control of sexually dimorphic social behaviors. *Curr. Opin. Neurobiol.* **38**, 89–95 (2016).
30. Zimmerman, C. A., Leib, D. E. & Knight, Z. A. Neural circuits underlying thirst and fluid homeostasis. *Nat. Rev. Neurosci.* **18**, 459–469 (2017).
31. Weber, F. & Dan, Y. Circuit-based interrogation of sleep control. *Nature* **538**, 51–59 (2016).
32. Arber, S. Motor circuits in action: specification, connectivity, and function. *Neuron* **74**, 975–989 (2012).

Acknowledgements We thank S. Sullivan for help with behaviour and mouse husbandry. E. Kremer (Montpellier) and R. Neve (MIT) provided viral vectors. E. Soucy and J. Greenwood helped design motivation assay. R. Hellmiss and K. Wilbur helped with illustrations. H. S. Knobloch-Bollmann provided advice on PVN cell types. We thank the members of the Dulac laboratory for comments on the manuscript. This work was supported by a Human Frontier Long-Term Fellowship, an EMBO Long-Term Fellowship and a Sir Henry Wellcome Fellowship to J.K., Fondation pour la Recherche Médicale grant SPE20150331860 to B.M.B., a NIH K99 Award and a NARSAD Young Investigator Award to A.E.A., a Howard Hughes Gilliam Fellowship to B.M.-R., a Harvard Mind Brain and Behavior faculty grant to N.U. and NIH grant 1R01HD082131-01A1 to C.D. C.D. and L.L. are investigators of the Howard Hughes Medical Institute.

Reviewer information *Nature* thanks V. Grinevich and the other anonymous reviewer(s) for their contribution to the peer review of this work.

Author contributions J.K. and C.D. conceived and designed the study. J.K performed and analysed tracing and optogenetics experiments. J.K. and B.M.B. performed and analysed photometry recordings. A.E.A. helped with in situ hybridization experiments, B.M.-R. helped with CTB tracing experiments, N.D.R. helped to analyse tracing data, and V.K. helped with optogenetics experiments. L.S.Z., K.M. and L.L. shared unpublished viral reagents. N.U. provided fibre photometry setup. J.K., B.M.B., N.D.R., A.E.A. and C.D. analysed and interpreted the results. J.K. and C.D. wrote the manuscript with input from all authors.

Competing interests The authors declare no competing interests.

Additional information
Extended data is available for this paper at https://doi.org/10.1038/s41586-018-0027-0.
Supplementary information is available for this paper at https://doi.org/10.1038/s41586-018-0027-0.
Reprints and permissions information is available at http://www.nature.com/reprints.
Correspondence and requests for materials should be addressed to C.D.
Publisher's note: Springer Nature remains neutral with regard to jurisdictional claims in published maps and institutional affiliations.

METHODS

Animals. The *Gal::cre* BAC transgenic line (Stock: Tg(Gal-cre)KI87Gsat/Mmucd, 031060-UCD) was imported from the Mutant Mouse Regional Resource Center and has previously been described[3]. Cre-dependent tdTomato reporter mice (*Gt(Rosa)26Sor*$^{tm9(CAGtdTomato)Hze}$)[33], C57BL/6J, OXT-IRES-Cre, Vgat-IRES-Cre and TH-IRES-Cre mice were obtained from Jackson Laboratories. Vglut2-IRES-Cre mice were provided by B. Lowell. The AVP-IRES-Cre line has previously been described[7]. CRH-IRES-Cre mice were obtained from B. Lowell, J. Majzoub and Jackson Laboratories. Animals were maintained on 12 h:12 h light:dark cycle (light on: 02:00–14:00) with food and water available ad libitum. Animal care and experiments were carried out in accordance with the NIH guidelines and approved by the Harvard University Institutional Animal Care and Use Committee (IACUC).

Histology and immunostaining. Animals were perfused transcardially with phosphate-buffered saline (PBS) followed by 4% paraformaldehyde (PFA) in PBS. Brains were dissected and post-fixed in 4% PFA for 16 h, then washed in PBS for 6 h. After embedding in 4% low-melting point agarose (Thermo Fisher, 16520-050) in PBS, 60-μm coronal sections were cut on a vibratome (Leica) and mounted on Superfrost Plus slides (VWR, 48311-703) with DAPI-containing VECTASHIELD mounting medium (Vector Laboratories, H-1200). For immunostaining in 48-well culture plates, sections were permeabilized for 30 min in PBS-T (0.3% Triton X-100 in PBS), post-fixed with PFA for 10 min, and washed in PBS-T (three times, 20 min each). Blocking was carried out overnight in blocking buffer (0.3% Triton X-100, 1% BSA, 2% normal donkey serum in PBS). Incubation with primary antibodies was performed for 24–48 h on a Nutator at 4 °C. After washing in PBS-T (five times, 60 min each), secondary antibodies were added for 48 h at 4 °C. After final washes in PBS-T (five times, 60 min each), sections were mounted. Primary antibodies: goat anti-Fos (Santa Cruz, sc-52, 1:500), chicken anti-GFP (Abcam, ab13970, 1:1,000), rabbit anti-AVP (Immunostar, 20069, 1:6,000), rabbit anti-OXT (Immunostar, 20068, 1:6,000). Secondary antibodies (all from Thermo Fisher): Alexa Fluor-568 anti-goat (A-11057, 1:1,500), Alexa Fluor-555 anti-goat (A-21432, 1:1,500) and Alexa Fluor-647 anti-goat (A-21447, 1:1,500). All antibodies were incubated in PBS-T, with the exception of Fos antibody, which was incubated in PBS.

RNA in situ hybridization. Freshly dissected brains were embedded in OCT (Tissue-Tek, 4583) and frozen with dry ice. Subsequently, 16-μm cryosections were collected on Superfrost Plus slides (VWR, 48311-703) and used for mRNA in situ hybridization. Fluorescent mRNA in situ hybridization was performed mostly as described[24]. Complementary DNA (cDNA) of *Gal* or *eYFP* mRNA was cloned in approximately 800-base-pair segments into a pCRII-TOPO vector (Thermo Fisher, K465040). Antisense complementary RNA (cRNA) probes were synthesized with T7 (Promega, P2075) or Sp6 polymerases (Promega, P1085) and labelled with digoxigenin (DIG, Roche 11175025910) or fluorescein (FITC, Roche 11685619910). Hybridization was performed with 0.5–1.0 ng ml^{-1} cRNA probes at 68 °C. Probes were detected using horseradish peroxidase (POD)-conjugated antibodies (anti-FITC-POD, Roche 11426346910, 1:250; anti-DIG-POD, Roche 11207733910, 1:500). Signals were amplified using biotin-conjugated tyramide (Perkin Elmer NEL749A001KT) and subsequently visualized with Alexa Fluor-488-conjugated streptavidin (Thermo Fisher, S11223) or the TSA-plus Cy3 system (Perkin Elmer, NEL744001KT).

Viruses. Recombinant AAV vectors were produced by the UNC Vector Core. AAV titres ranged from 1.3 to 2.6 × 10^{12} viral particles ml^{-1}, based on quantitative PCR analysis. Pseudotyped, G-deleted rabies virus[4] was obtained from the Salk vector core at a titre of 4.3 × 10^{8} viral particles ml^{-1}. The pAAV-CAG-FLEx-Syn-GFP plasmid was provided by S. Arber and AAV1/CAG-FLEx-Syn-GFP was produced by the UNC Vector Core. The pAAV-CAG-FLEx-TCB, pAAV-CAG-FLEx-RG[34], pAAV-CAG-FLEx^{FRT}-TC and pAAV-CAG-FLEx^{FRT}-RG plasmids were provided by L.L. (Stanford University), and AAV5/DJ-hSyn1-FLEx^{FRT}-mGFP[35]; AAV1/CAG-FLEx^{FRT}-TC and AAV1/CAG-FLEx^{FRT}-RG were packaged by the UNC Vector core. L.L. and E. Kremer provided CAV2-FLEx^{loxP}-Flp. L.S.Z. provided CAV2-FLEx-ZsGreen. AAV1/CAG-FLEx-tdTomato, AAV1/Syn-FLEx-GCaMP6m, AAV5/EF1α-DIO-hChR2(H134R)-eYFP and AAV5/EF1α-DIO-eYFP were purchased from UPenn Vector core. HSV-hEF1α-LSL1-GCaMP6m (HT) was obtained from MIT Vector Core.

Anterograde tracing. Anterograde tracing experiments were performed in *Gal::cre* mice (or in C57BL/6J for control experiments) at around 8–12 weeks of age. All surgeries were performed under aseptic conditions in animals anaesthetized with 100 mg kg^{-1} ketamine (KetaVed, Vedco) and 10 mg kg^{-1} xylazine (AnaSed) via intraperitoneal (i.p.) injection. Using a Nanoject II injector (Drummond Scientific), 300 nl of a 1:1 mixture of AAV1/CAG-FLEx-tdTomato:AAV1/CAG-FLEx-Syn-GFP[36] (synaptophysin–GFP) was injected into the MPOA (coordinates: anteroposterior (AP): 0.0 mm from Bregma; mediolateral (ML): −0.5 mm from the midline, dorsoventral (DV): −5.05 mm) to visualize presynaptic terminals of MPOA^{Gal} neurons. Syn–GFP was chosen to distinguish presynaptic sites from fibres of passage. Analgesia (buprenorphine, 0.1 mg kg^{-1}, i.p.) was administered for two days after each surgery. Two weeks later, mice were euthanized and dissected. In some experiments, a 1:1 mixture of AAV1/CAG-FLEx-tdTomato:AAV1/CAG-FLEx-Syn-GFP was injected to visualize presynaptic terminals of MPOA^{Gal} neurons. For quantification of synaptic density, the average pixel intensity in a target region containing presynaptic GFP^{+} punctae was calculated and the background was subtracted. Because injections were unilateral and no labelling was observed in most cases contralaterally, the equivalent region on the contralateral hemisphere was chosen for background subtraction; in cases where contralateral GFP^{+} punctae were present, an adjacent unlabelled region was chosen. Background-corrected intensities were normalized to the average pixel intensity at the MPOA injection site for each brain.

Trans-synaptic retrograde tracing. Input tracing experiments were performed in *Gal::cre* mice (or C57BL/6J in control experiments) at about 8–12 weeks of age. We injected 150–200 nl of a 1:1 mixture of AAV1/CAG-FLEx-TC^{B}:AAV1/CAG-FLEx-RG unilaterally into the MPOA. Two weeks later, 450–600 nl EnvA-pseudotyped, RG-deleted, GFP-expressing rabies virus (EnvA-ΔG-rabies) was injected into the MPOA. After recovery, mice were housed in a biosafety-level-2 (BL2) facility for four days before euthanization. Relative input strength was quantified from brain sections as follows: every second 60-μm section was imaged and cells were counted using the ImageJ CellCounter plugin. GFP^{+} cells on the injected hemisphere were counted and assigned to brain areas based on classifications of the Paxinos Mouse Brain Atlas[37], using anatomical landmarks in the sections visualized by DAPI staining and tissue autofluorescence. In addition, all contralateral and non-assigned GFP^{+} cells were counted to obtain the total number of GFP^{+} cells. We then quantified the number of ipsilateral mCherry^{+} starter neurons per brain area and the total number of starter neurons. Because starter neurons are both GFP^{+} and mCherry^{+}, whereas presynaptic neurons are only GFP^{+}, the total number of starter neurons was subtracted from the total number of GFP^{+} neurons to obtain the total number of presynaptic neurons within the MPOA. Finally, the relative input fraction for each area was determined by dividing the number of presynaptic neurons detected in that brain area by the total number of presynaptic neurons in a given brain. Injection of starter AAVs and EnvA-ΔG-rabies into the MPOA *of C57BL/6J* mice did not result in detectable background labelling (Extended Data Fig. 5a). Inputs from PAG were detected only in a subset of animals. Presynaptic AVP^{+} neurons in the PVN were identified as predominantly magnocellular based on cell body size[38,39] and position[40]. Presynaptic neurons in the MPOA (Fig. 2d–g and Extended Data Fig. 2e–j) were identified as Gal^{+} by in situ hybridization.

Lateralization effects. Retrograde and anterograde tracing experiments were performed in the right hemisphere. However, a recent study found that the oxytocin receptor is more highly expressed in the left auditory cortex of females and that OXT binding there is crucial for pup retrieval[5]. We therefore investigated potential lateralization effects by tracing MPOA^{Gal} neurons in the left hemisphere. Resulting presynaptic neuron numbers and projection patterns (Extended Data Figs. 1b, 2c) were indistinguishable from those obtained after right-hemispheric tracing, suggesting that anatomical lateralization is not a dominant feature of the subcortical circuits described here.

Projection-specific trans-synaptic retrograde tracing. For projection-specific trans-synaptic retrograde tracing (cTRIO (cell-type-specifically tracing the relationship between input and output))[12], 300–500 nl of CAV2-FLEx^{loxP}-Flp was injected into identified target areas of MPOA^{Gal} neurons (for coordinates, see Extended Data Table 1) in 8–12-week-old *Gal::cre* mice. During the same surgery, 300–600 nl of a 1:1 mixture of AAV1/CAG-FLEx^{FRT}-TC:AAV1/CAG-FLEx^{FRT}-RG[12] (starter AAVs) was injected into the MPOA. This combination of Cre-dependent, Flp-expressing CAV and Flp-dependent starter AAVs renders MPOA^{Gal} neurons projecting to a specific target area susceptible to subsequent infection with G-deleted, EnvA-pseudotyped rabies virus. Two weeks later, 450–500 nl of EnvA-ΔG-rabies was injected into the same MPOA coordinate. After recovery, mice were housed in a biosafety-level-2 (BL2) facility for four days before euthanization. Injection of starter AAVs without CAV did not result in expression (Extended Data Fig. 5b, c). However, because the injection of all cTRIO tracing viruses into C57BL/6J mice resulted in background expression near the injection site (Extended Data Fig. 5d), the following areas were excluded from analysis: MPOA, BNST, AH, PVN and supraoptic nucleus (SON). This background labelling is probably due to low levels of Cre- or Flp-independent expression of TVA-mCherry and RG[12].

We quantified the connectivity of each MPOA^{Gal} projection to its inputs using a multinomial regression model (response: neuron counts in each input area, factors: MPOA^{Gal} projections). The baseline category in the model was represented by the mean input fraction across all experiments. Reported effects are therefore relative to a randomly chosen projection and the *P* values reported in Fig. 2k, l are obtained from a normal distribution in which the *z* scores are the effects of the multinomial regression divided by their corresponding standard errors. To test for differences in the multinomial distribution of input to target region projections, the least-square

means from the multinomial regression model was computed using the lsmeans package in R and used to run all pairwise comparisons.

MPOA^{Gal} input activity screen. To determine which fraction of MPOA^{Gal} inputs is activated during parental behaviour, viral injections were performed as described in 'Trans-synaptic retrograde tracing'. Animals were single-housed until behavioural testing four days later with two pups (see 'Parental behaviour assay'). For the equivalent experiments in mothers and fathers, 8–12-week-old *Gal::cre* males and females were paired up 10 days before injection of starter viruses and returned to their home cage where they remained until three days after injection of EnvA-ΔG-rabies when either the father and litter (for testing of mothers) or the mother and litter (for testing of fathers) were removed from the home cage. Parents underwent behavioural testing on the following day, that is, four days after injection of EnvA-ΔG-rabies. Typically around 80% of virgin females and more than 90% of mothers and fathers were parental. Ninety minutes after onset of retrieval, mice were deeply anaesthetized with isoflurane and rapidly perfused transcardially with 30 ml of ice-cold PBS, followed by 30 ml of ice-cold PFA (4% in PBS). Brains were dissected and post-fixed in PFA (4% in PBS) at 4 °C for 16 h. On the next day, brains were rinsed with cold PBS and 60-μm coronal sections were prepared with a vibratome (Leica VT1000 S). Sections were further post-fixed in PFA (4% in PBS) at room temperature for 10 min and immunostaining against Fos was performed (see 'Histology and immunostaining'). Only brains from mice that performed all steps of pup-directed parental behaviour (sniffing, retrieval, grooming, licking, crouching) were processed. Animals that were habituated in the test arena but not exposed to pups served as negative controls. Unpaired *t*-tests were used to assess activation of input areas between parental and control animals and *P* values were adjusted for multiple comparisons using the Benjamini–Hochberg method (false-discovery rate (FDR) < 0.05).

Previous studies have reported that the basic properties of ΔG-rabies-infected neurons are not altered until seven days after infection[41,42] and likewise, effects of rabies on (transgene) expression levels have only been reported seven days after infection[43]. Because animals were tested and perfused four days after rabies infection in our study, neuronal physiology and Fos activation should be mostly unaffected. Because we reliably observed Fos immunostaining in rabies$^+$ neurons (Fig. 1g–j), rabies infection per se does not preclude activity-dependent Fos expression after four days. However, rabies infection could theoretically upregulate Fos expression in infected neurons, resulting in an overestimation of activated input neurons in our dataset. To address this possibility, we compared Fos$^+$ cell numbers in the MPOA of unilaterally rabies-injected mothers between the injected (ipsilateral) and the non-injected (contralateral) hemisphere (Extended Data Fig. 1c, top). We found that numbers of Fos$^+$ neurons were not significantly different between hemispheres (Extended Data Fig. 1c, bottom; $P = 0.43$; paired *t*-test; $n = 6$). Therefore, rabies infection is unlikely to strongly affect Fos$^+$ expression in our experimental paradigm.

MPOA^{Gal} projection activity screen. To determine the activation of individual MPOA^{Gal} projections during parental behaviour, 300–500 nl of CAV2-FLEx-ZsGreen was injected into identified MPOA^{Gal} target areas in 8–12-week-old *Gal::cre* females. Animals were single-housed one week after injection. Behavioural testing with two pups (see 'Parental behaviour assay') was performed three weeks after injection to allow for efficient retrograde transport of the virus. For the equivalent experiments in fathers, 8–10-week-old *Gal::cre* virgin males were individually paired up with females for four days, injected and subsequently returned to the female. Two to three days after pups were born (around three weeks after injection), and one day before testing, the female and pups were removed from the cage. Testing, brain collection and immunostaining were performed as described in 'MPOA^{Gal} input activity screen'. Because MPOA^{Gal} neurons are not activated in non-pup-exposed mice[3], negative controls were not performed in these experiments.

Axon collateralization experiments. In order to assess axon collateralization of MPOA^{Gal} neurons (Extended Data Fig. 4), *Gal::cre* mice received injections of 300–500 nl of CAV-FLEx^{loxP}-Flp into an MPOA^{Gal} target site (for coordinates, see Extended Data Table 1) and of 600 nl of AAV5/hSyn1-FLEx^{FRT}-mGFP into the MPOA. Mice were euthanized eight weeks later and the signal was amplified by anti-GFP immunostaining.

CTB tracing. Mice expressing tdTomato in Gal$^+$ neurons (*Gal::cre*$^{+/-}$*loxP-Stop-loxP-tdTomato*$^{+/-}$) received pairwise injections of 50–100 nl of 0.5% (wt/vol) fluorescently labelled cholera toxin B subunit (CTB-488, Thermo Fisher C22841, CTB-647, Thermo Fisher C34778). After seven days, brains were collected, fixed and 60-μm sections prepared. Individual sections were fixed again in 4% PFA for 10 min. The fraction of double-labelled, tdTomato$^+$, Gal$^+$ neurons in the MPOA was quantified. In control experiments, a 1:1 mixture of CTB-488 and CTB-647 was injected into MeA or PAG.

Imaging and image analysis. Samples were imaged using an Axio Scan.Z1 slide scanner (Zeiss), and confocal stacks were acquired on an LSM 880 confocal microscope (Zeiss). Image processing was performed using custom routines for the Fiji distribution of ImageJ. For most tracing experiments, every second section was imaged, with the exception of MPOA^{Gal} projection activity and CTB-tracing experiments, where every MPOA-containing section was imaged and analysed.

Parental behaviour assay. Before behavioural testing animals were housed individually for 5–7 days unless otherwise specified. Experiments started at the beginning of the dark phase and were performed under dim red light. Testing was performed in the home cage (with the exception of locomotion assays, see below) and preceded by a 30-min habituation period. Two 1–4-day-old C57BL/6J pups were placed in different corners opposite the nest. Once retrieval occurred, a timer was started. Each test was recorded using a multi-camera surveillance system (GeoVision GV-1480) and behaviours were scored by an individual blind to the genotype using the Observer 5.0 or XT 8 software (Noldus Information Technology).

Fibre photometry. Fibre photometry (fluorometry) was performed as previously described[44]. For photometry recordings, 8–12-week-old *Gal::cre*$^{+/-}$*loxP-Stop-loxP-tdTomato*$^{+/-}$ mice were used. For pan-MPOA^{Gal} recordings, 400–500 nl of AAV1/Syn-FLEx-GCaMP6m (Upenn Vector Core) was injected into the MPOA; for projection-specific recordings, 600–700 nl of hEF1α-LS1L-GCaMP6m, a Cre-dependent, retrograde, long-term herpes simplex virus (LT-HSV) was bilaterally injected into MPOA^{Gal} target areas. During the same surgery, a custom 400-μm fibre-optic cannula (Doric Lenses) was implanted into the MPOA (for coordinates, see Extended Data Table 1). For recordings in mothers and fathers, animals were paired up five days before surgery, to ensure that pups were born around three weeks after virus injection. One day after surgery, animals were returned to their mating partner. The implanted animal's mating partner and offspring were removed 3–5 h before recordings. Virgin female mice were single-housed seven days before the first recording session and thereafter between experiments. Recordings were made 2–4 weeks after the surgery under IR illumination in the home cage of the mouse. Mice were briefly (around 10 min) habituated in the recording setup before 8–10 pups (1–4 days old) were introduced into the cage. Recording sessions typically lasted 10–20 min, with at least two days between sequential recordings. The implant was coupled to a custom patch cord (Doric Lenses) to simultaneously deliver 473-nm excitation light from a DPSS laser (Opto Engine LLC), passed through a neutral density filter (4.0 optical density, Thorlabs) and to collect fluorescence emission. Activity-dependent fluorescence emitted by cells in the vicinity of the implanted fibre tip was collected by a 0.65 NA microscope objective (Olympus), spectrally separated from the excitation light using a dichroic mirror (Chroma), passed through a band pass filter (ET500/50, Chroma) and focused onto a photodetector (FDS10X10, Thorlabs) connected to a current preamplifier (SR570, Stanford Research Systems). Another band pass filter (ET600/20) in front of a second photodetector/preamplifier was used to collect tdTomato fluorescence. Owing to considerable bleed-through of the GCaMP signal into the tdTomato channel, we chose not to use the tdTomato recording trace to normalize our data, instead opting for a set of behavioural controls for motion artefacts (see below). The preamplifier output voltage signal was collected by a NIDAQ board (PCI-e6321, National Instruments) connected to a computer running LabVIEW (National Instruments) for signal acquisition. Video recordings were acquired at 15 frames per second and the signal from the optical fibre was sampled at 1 kHz. A TTL-triggered photodiode next to the cage was used to align videos and voltage recording traces.

Analysis was performed using custom MATLAB (MathWorks) routines. Only recordings with a stable baseline were included in our analysis. The raw signal over each entire recording session was divided by the mean of a Gaussian fit to the distribution of GCaMP to normalize the baseline over the recording session. Since the increase in GCaMP signal preceded event detection in some cases (for example, see Fig. 3c), *z* scores were calculated using the period from −5 to −2 s before event detections as baseline and from 0 to 3 s from event detection as signal. For statistical analyses (that is, *t*-tests, ANOVA), we considered a value of $P \leq 0.05$ significant. Behaviours were scored manually off-line by an experimenter blind to the photometry recording data. The responses to a stimulus type within a session (typically 5–10 trials per behaviour type) were averaged, and these session averages across mice were used as data displayed in Fig. 3 and Extended Data Fig. 6.

We performed a set of behavioural controls to address the possible contribution of motion artefacts to the recorded signal. In all of the following cases, (orofacial) motor actions highly identical to pup interactions did not result in detectable increases in GCaMP fluorescence intensity. No increase in signal was observed when animals retrieved or sniffed a pup-sized cracker (Fig. 3j), during eating (Fig. 3k) or during self-grooming (Fig. 3l). In addition, no increase in signal was detectable when animals retrieved bedding material to the nest (Fig. 3h). Finally, chemoinvestigation of accessible versus inaccessible pups resulted in different GCaMP responses (from −5 to 0 s period before sniffing, Extended Data Fig. 6i, j). Therefore, the increases in signal intensity observed during pup interactions very probably represent actual activity changes rather than motion artefacts.

Optogenetics. *Gal::cre* mice 8–12 weeks of age were used in these experiments. Because potential increases in parental behaviour would be difficult to detect in already highly parental mothers and fathers, we performed these experiments in virgin animals, in which a higher dynamic range of parental interactions can be assessed. Animals were exposed to two pups in their home cage (see 'Parental behaviour assay') and those that attacked (virgin males) or initiated parental behaviour (virgin females) within 15 min were selected for surgery. We injected 700 nl of AAV5/EF1α-DIO-hChR2(H134R)-eYFP (activation) or AAV5/EF1α-DIO-eNpHR3.0-eYFP (inhibition) bilaterally into the MPOA and in the same surgery a dual fibre-optic cannula (300 μm, 0.22 NA, Doric Lenses) was implanted 0.4–0.5 mm above the respective $MPOA^{Gal}$ projection target (Extended Data Table 1) and affixed to the skull with dental cement. Mice were tested 3–5 weeks after injection to allow for efficient expression of ChR2 or eNpHR3.0 into axon terminals. On testing day, the implant was connected to an optical fibre attached to either a 473-nm laser (150 mW, Laserglow Technologies) or a 460-nm LED (50 W, Prizmatix) for optogenetic activation, or a 589-nm laser (300 mW, Opto Engine LLC) for inhibition, via a commutator. Animals were tested in either stimulation or non-stimulation trials in randomized order, with two days between trials. In addition, the order in which animals were tested during each experimental session was randomized. In pup exposure experiments, two C57BL/6J pups, 1–3 days of age, were introduced to the test animal's home cage in each corner furthest from the nest after 10 min of habituation. For activation experiments, blue light (473 nm) was delivered in 20-ms pulses at 20 Hz for 1–4 s whenever the animal contacted a pup with its snout. The light power exiting the fibre tip was 5 mW, which we calculated as providing an irradiance of 5–10 mW mm^{-2} at the target region (using the brain tissue light transmission calculator provided by the Deisseroth laboratory, http://www.stanford.edu/group/dlab/cgi-bin/graph/chart.php). For loss-of-function experiments, constant yellow light (589 nm) was delivered at 8–10 mW at the fibre tip, amounting to an estimated irradiance of 15–20 mW mm^{-2} at the target. Each trial lasted up to 10 min but when virgin males attacked and wounded a pup, the trial was ended and the pup was euthanized.

The following behaviours were scored and quantified: pup sniffing, grooming and licking, pup retrieval to the nest, aggression (animal grabs the pup violently and attempts to bite), crouching (animal hovers above the pup in the nest), nest building and time spent in the nest. For the motivation assay, following a 10-min habituation period a transparent barrier was inserted into the home cage, dividing the cage into a nest and a pup compartment. Next, 4–5 pups were introduced into the pup compartment and 473-nm light was delivered in 20-ms pulses at 20 Hz for 4 s every 10 s for a total of 6 min. Locomotion was assessed in a 36 × 25-cm arena over a period of 5 min. In stimulation trials, 473 nm light (20 ms, 20 Hz) was delivered to the implant for 4 s every 20 s, equivalent to the stimulation administered during a typical pup interaction trial. The position of the animal was tracked and analysed by Ethovision XT 8 software (Noldus) to calculate the average velocity and moved distance. For intruder assays, an 8–12-week-old C57BL/6J intruder of the opposite sex (receptive virgin female, as determined by vaginal smear, or sexually experienced male) was introduced into the resident mouse cage and 473-nm light was delivered in 20-ms pulses at 20 Hz for 1–4 s whenever the animal contacted the intruder with its snout. Sniffing and grooming durations were scored over a period of 5 min, aggression was scored during a 10-min period. After behavioural testing, animals were transfused transcardially and fibre placement as well as efficient light transmission were verified.

Statistics and reproducibility. Data were analysed by two-tailed, unpaired or paired Student's *t*-test, by two-tailed Fisher's exact test or by χ^2 test if not indicated otherwise, using Graph Pad Prism 7 for Mac OS, MATLAB or R. Statistical details are given in the respective figure legends. Experiments were independently performed twice (Figs. 1b–f, 2e–g, k, l, 3c–l, 4 and Extended Data Figs. 1, 2a–d, i, j, 3d, e, 4b–f, 7, 8), three (Figs. 1g–j, F2b, c, h, i, 3n–p and Extended Data Fig. 6b–d) or four times (Extended Data Fig. 6f–h).

Reporting Summary. Further information on experimental design is available in the Nature Research Reporting Summary linked to this paper.

Code availability. The code that supports the findings of this study is available from the corresponding author upon request.

Data availability. The data that support the findings of this study are available from the corresponding author upon request.

33. Madisen, L. et al. A robust and high-throughput Cre reporting and characterization system for the whole mouse brain. *Nat. Neurosci.* **13**, 133–140 (2010).
34. Miyamichi, K. et al. Dissecting local circuits: parvalbumin interneurons underlie broad feedback control of olfactory bulb output. *Neuron* **80**, 1232–1245 (2013).
35. Beier, K. T. et al. Circuit architecture of VTA dopamine neurons revealed by systematic input–output mapping. *Cell* **162**, 622–634 (2015).
36. Esposito, M. S., Capelli, P. & Arber, S. Brainstem nucleus MdV mediates skilled forelimb motor tasks. *Nature* **508**, 351–356 (2014).
37. Franklin, K. B. J. & Paxinos, G. *The Mouse Brain in Stereotaxic Coordinates* 3rd edn (Academic, New York, 2007).
38. Eliava, M. et al. A new population of parvocellular oxytocin neurons controlling magnocellular neuron activity and inflammatory pain processing. *Neuron* **89**, 1291–1304 (2016).
39. Xiao, L., Priest, M. F., Nasenbeny, J., Lu, T. & Kozorovitskiy, Y. Biased oxytocinergic modulation of midbrain dopamine systems. *Neuron* **95**, 368–384 (2017).
40. Swanson, L. W. & Sawchenko, P. E. Hypothalamic integration: organization of the paraventricular and supraoptic nuclei. *Annu. Rev. Neurosci* **6**, 269–324 (1983).
41. Wickersham, I. R., Finke, S., Conzelmann, K. K. & Callaway, E. M. Retrograde neuronal tracing with a deletion-mutant rabies virus. *Nat. Methods* **4**, 47–49 (2007).
42. Osakada, F. et al. New rabies virus variants for monitoring and manipulating activity and gene expression in defined neural circuits. *Neuron* **71**, 617–631 (2011).
43. Weible, A. P. et al. Transgenic targeting of recombinant rabies virus reveals monosynaptic connectivity of specific neurons. *J. Neurosci.* **30**, 16509–16513 (2010).
44. Menegas, W., Babayan, B. M., Uchida, N. & Watabe-Uchida, M. Opposite initialization to novel cues in dopamine signaling in ventral and posterior striatum in mice. *eLife* **6**, e21886 (2017).
45. Sukikara, M. H., Mota-Ortiz, S. R., Baldo, M. V., Felicio, L. F. & Canteras, N. S. The periaqueductal gray and its potential role in maternal behavior inhibition in response to predatory threats. *Behav. Brain Res.* **209**, 226–233 (2010).
46. Fleming, A. S., Vaccarino, F. & Luebke, C. Amygdaloid inhibition of maternal behavior in the nulliparous female rat. *Physiol. Behav.* **25**, 731–743 (1980).
47. Numan, M., Numan, M. J. & English, J. B. Excitotoxic amino acid injections into the medial amygdala facilitate maternal behavior in virgin female rats. *Horm. Behav.* **27**, 56–81 (1993).
48. Sheehan, T., Paul, M., Amaral, E., Numan, M. J. & Numan, M. Evidence that the medial amygdala projects to the anterior/ventromedial hypothalamic nuclei to inhibit maternal behavior in rats. *Neuroscience* **106**, 341–356 (2001).
49. Insel, T. R. & Harbaugh, C. R. Lesions of the hypothalamic paraventricular nucleus disrupt the initiation of maternal behavior. *Physiol. Behav* **45**, 1033–1041 (1989).
50. Numan, M. & Corodimas, K. P. The effects of paraventricular hypothalamic lesions on maternal behavior in rats. *Physiol. Behav.* **35**, 417–425 (1985).
51. Lee, G. & Gammie, S. C. $GABA_A$ receptor signaling in the lateral septum regulates maternal aggression in mice. *Behav. Neurosci* **123**, 1169–1177 (2009).
52. D'Anna, K. L. & Gammie, S. C. Activation of corticotropin-releasing factor receptor 2 in lateral septum negatively regulates maternal defense. *Behav. Neurosci* **123**, 356–368 (2009).
53. Hansen, S., Harthon, C., Wallin, E., Löfberg, L. & Svensson, K. Mesotelencephalic dopamine system and reproductive behavior in the female rat: effects of ventral tegmental 6-hydroxydopamine lesions on maternal and sexual responsiveness. *Behav. Neurosci.* **105**, 588–598 (1991).
54. Hansen, S. Maternal behavior of female rats with 6-OHDA lesions in the ventral striatum: characterization of the pup retrieval deficit. *Physiol. Behav.* **55**, 615–620 (1994).
55. Li, M. & Fleming, A. S. The nucleus accumbens shell is critical for normal expression of pup-retrieval in postpartum female rats. *Behav. Brain Res.* **145**, 99–111 (2003).
56. Keer, S. E. & Stern, J. M. Dopamine receptor blockade in the nucleus accumbens inhibits maternal retrieval and licking, but enhances nursing behavior in lactating rats. *Physiol. Behav.* **67**, 659–669 (1999).
57. Numan, M. et al. The effects of D1 or D2 dopamine receptor antagonism in the medial preoptic area, ventral pallidum, or nucleus accumbens on the maternal retrieval response and other aspects of maternal behavior in rats. *Behav. Neurosci.* **119**, 1588–1604 (2005).
58. Numan, M. & Nagle, D. S. Preoptic area and substantia nigra interact in the control of maternal behavior in the rat. *Behav. Neurosci.* **97**, 120–139 (1983).
59. Bridges, R. S., Mann, P. E. & Coppeta, J. S. Hypothalamic involvement in the regulation of maternal behaviour in the rat: inhibitory roles for the ventromedial hypothalamus and the dorsal/anterior hypothalamic areas. *J. Neuroendocrinol.* **11**, 259–266 (1999).
60. Numan, M. & Numan, M. A lesion and neuroanatomical tract-tracing analysis of the role of the bed nucleus of the stria terminalis in retrieval behavior and other aspects of maternal responsiveness in rats. *Dev. Psychobiol.* **29**, 23–51 (1996).
61. Numan, M., Rosenblatt, J. S. & Komisaruk, B. R. Medial preoptic area and onset of maternal behavior in the rat. *J. Comp. Physiol. Psychol.* **91**, 146–164 (1977).
62. Bridges, R. S., Numan, M., Ronsheim, P. M., Mann, P. E. & Lupini, C. E. Central prolactin infusions stimulate maternal behavior in steroid-treated, nulliparous female rats. *Proc. Natl Acad. Sci. USA* **87**, 8003–8007 (1990).
63. Numan, M. & Numan, M. J. Projection sites of medial preoptic area and ventral bed nucleus of the stria terminalis neurons that express Fos during maternal behavior in female rats. *J. Neuroendocrinol.* **9**, 369–384 (1997).
64. Lonstein, J. S., Simmons, D. A., Swann, J. M. & Stern, J. M. Forebrain expression of *c-fos* due to active maternal behaviour in lactating rats. *Neuroscience* **82**, 267–281 (1997).

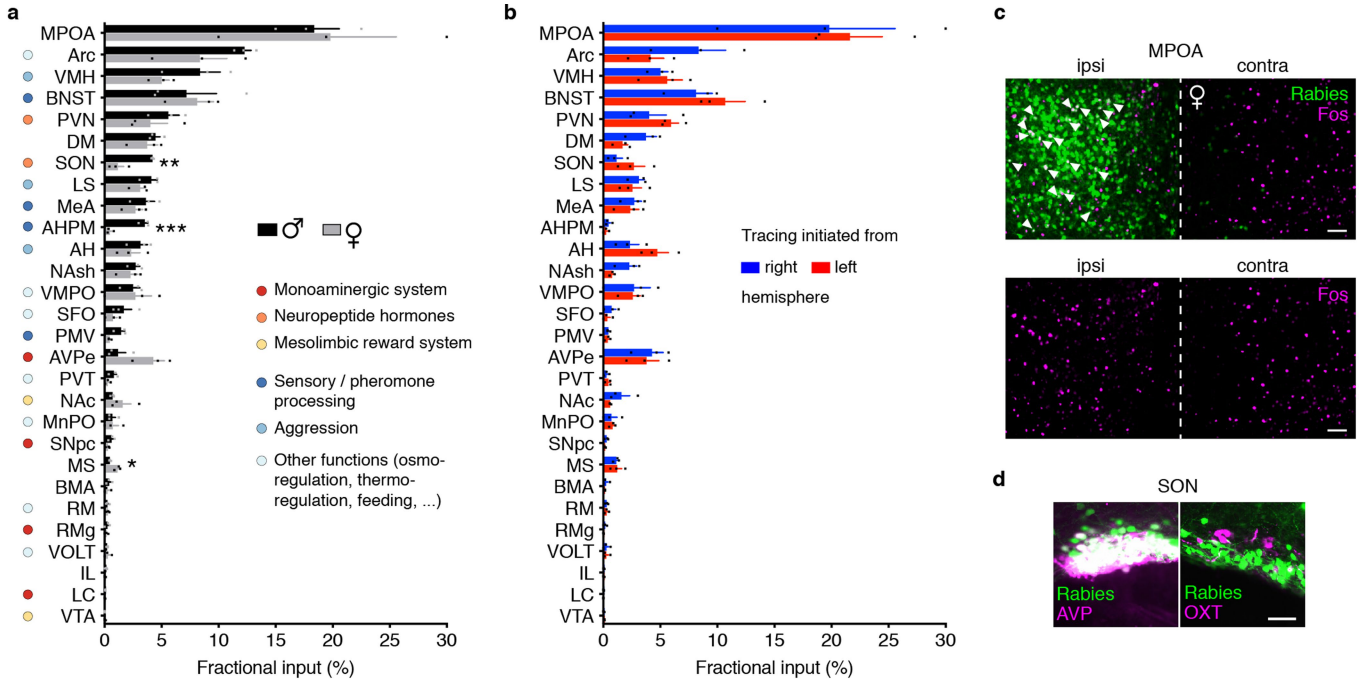

Extended Data Fig. 1 | Putative functional roles of brain areas providing monosynaptic inputs into MPOA^{Gal} neurons. a, Comparison between MPOA^{Gal} input fractions in virgin males ($n = 3$) and virgin females ($n = 3$) after rabies tracing (see Fig. 1a). Sexually dimorphic inputs are highlighted. Two-tailed t-tests, supraoptic nucleus (SON), $^{**}P = 0.0041$; posteriomedial amygdalo-hippocampal area (AHPM), $^{***}P = 0.0007$; medial septum (MS), $^{*}P = 0.0133$. **b**, Comparison between MPOA^{Gal} input fractions after rabies tracing was initiated from the right ($n = 3$) or left ($n = 3$) hemisphere in virgin females. No significant differences were found ($P > 0.05$; two-tailed paired t-test). **c**, Comparison between rabies-injected (ipsilateral (ipsi)) and non-injected (contralateral (contra)) MPOA of a mother after parental behaviour. Activated (Fos^{+}) rabies^{+} neurons are shown (top, arrowheads). Fos^{+} neuron numbers are not significantly different between hemispheres (bottom, $P = 0.43$, 95% confidence interval −4.176–1.843; two-tailed paired t-test; $n = 6$). **d**, MPOA^{Gal} neurons receive monosynaptic inputs from magnocellular SON^{AVP} neurons (mothers, 72.7 ± 9.3% overlap, $n = 3$; virgin females, 77.4 ± 4.3%, $n = 3$; fathers, 83.3 ± 3.3%, $n = 3$) but rarely from SON^{OXT} neurons (mothers, 4.6 ± 4.2% overlap, $n = 2$; virgin females, 4.5 ± 1.0%, $n = 2$; fathers, 2.8 ± 1.8%, $n = 2$). Data are mean ± s.e.m. Scale bars, 100 μm (**c**) and 50 μm (**d**).

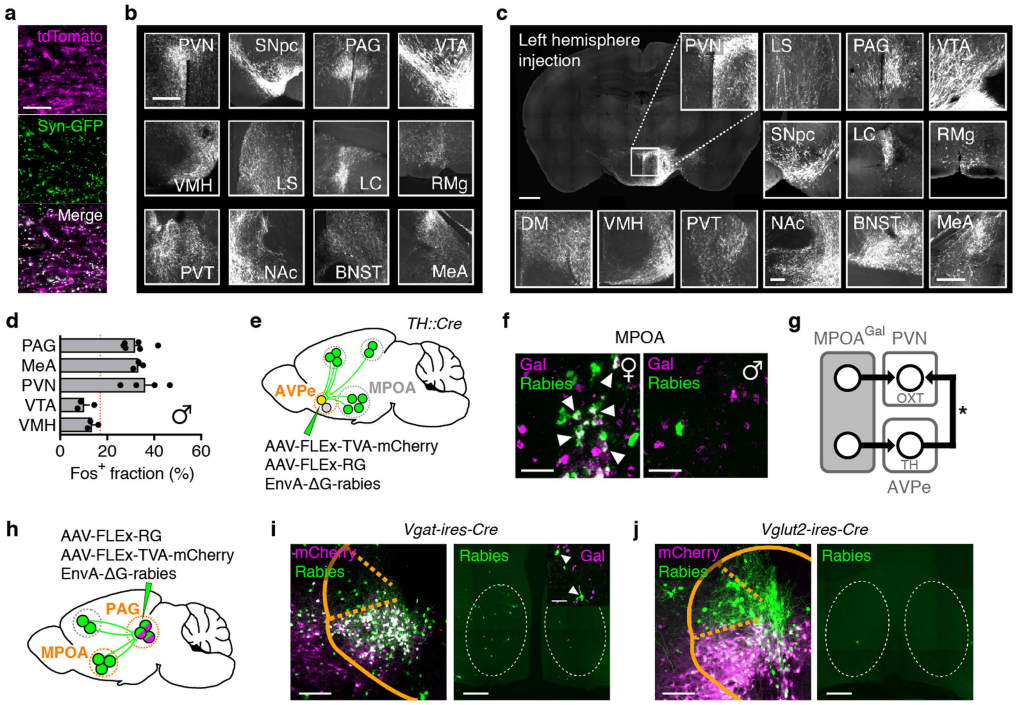

Extended Data Fig. 2 | MPOA^{Gal} projections in males and downstream connectivity. a, Synaptophysin–GFP (Syn–GFP) labelling of presynaptic sites in MPOA^{Gal} projections. **b**, Representative MPOA^{Gal} projections from a virgin male, identified by tdTomato fluorescence. **c**, Representative MPOA^{Gal} projections, identified by tdTomato fluorescence, after viral injection into the left MPOA. **d**, Fos^{+} fractions of virally labelled MPOA^{Gal} projections in fathers ($n = 6, 3, 4, 3, 3$, respectively, from top to bottom). Red line depicts the population average[3]. Data are mean ± s.e.m. **e**, Trans-synaptic retrograde rabies tracing from AVPeTH neurons. **f**, MPOA^{Gal} neurons presynaptic to AVPeTH neurons in females (left, indicated by arrowheads, 21.4% Gal^{+} neurons, 47 out of 220 neurons, $n = 3$) and males (right, 16.7% Gal^{+}, 4 out of 24 neurons, $n = 2$). **g**, Direct and indirect MPOA^{Gal} to PVN^{OXT} connectivity. Asterisk, AVPeTH neurons form excitatory synapses with PVN^{OXT} neurons in females[11]. **h**, Conditional monosynaptic retrograde tracing initiated from PAG. **i**, **j**, Injection sites with mCherry^{+} starter neurons in PAG of Vgat-IRES-Cre (**i**, left) or Vglut2-IRES-Cre (**j**, left) mice. Presynaptic, rabies^{+}Gal^{+} neurons are detected in MPOA when tracing is initiated from PAG^{Vgat} (**i**, right, indicated by arrowheads), but not PAG^{Vglut2} (**j**, right), neurons. Scale bars, 50 μm (**a**, **f** and **i**, inset), 200 μm (**i** and **j**, left) 250 μm (**b**, **c**, inset and **i** and **j**, right) and 500 μm (**c**, left).

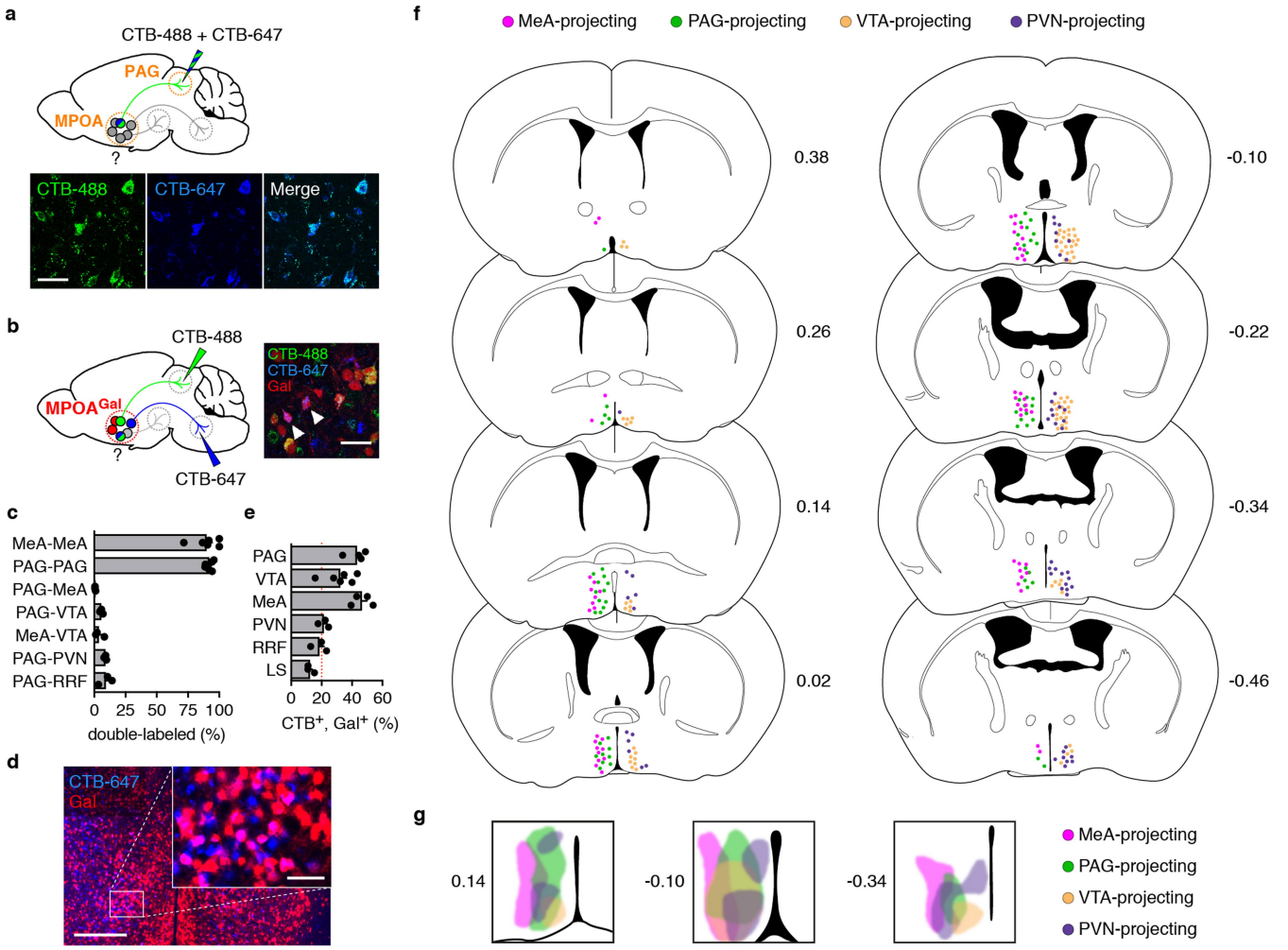

Extended Data Fig. 3 | MPOA^{Gal} projections correspond to mostly non-overlapping neuronal subpopulations. a, Control injection of a 1:1 mixture of CTB-488 and CTB-647 into PAG results in highly overlapping neuron populations in the MPOA (quantification in **c**). **b**, Strategy to determine collaterals between pairwise injected MPOA^{Gal} projections in *Gal::cre*$^{+/-}$*loxP-Stop-loxP-tdTomato*$^{+/-}$ mice. An example with two double-labelled MPOA^{Gal} neurons is shown after injection of CTB-488 into PAG and CTB-647 into VTA (right, indicated by arrowheads). **c**, Quantification of data in **a**, **b**. Data are mean ± s.e.m. ($n = 6, 6, 3, 3, 3, 3, 3$, respectively, from top to bottom). **d**, Representative image from MPOA of *Gal::cre*$^{+/-}$*loxP-Stop-loxP-tdTomato*$^{+/-}$ mouse after injection of CTB-647 into PAG. Note high overlap between Gal$^+$ and CTB$^+$ neurons. **e**, Frequency of Gal$^+$ neurons in individual, CTB-labelled MPOA projections ($n = 4, 6, 4, 3, 3, 3$, respectively, from top to bottom). Red line depicts expected labelling frequency, based on proportion of Gal$^+$ MPOA neurons[3] (around 20%). **c**, **e**, Data are mean ± s.e.m. **f**, Distribution of cell bodies corresponding to specific MPOA^{Gal} projections. Individual MPOA^{Gal} projection areas in *Gal::Cre* virgin females were injected with Cre-dependent CAV2-FLEx-ZsGreen (see Fig. 2h). Only labelling patterns on the ipsilateral, injected side are shown and only two projection-specific subpopulations per side are displayed for clarity. Mouse brain images in this figure have been reproduced with permission from Elsevier[37]. **g**, Zones occupied by MPOA^{Gal} cell bodies projecting to MeA, PAG, VTA and PVN in anterior (left), central (middle) and posterior (right) MPOA. **f**, **g**, Distance from bregma is shown in mm. Scale bars, 50 μm (**a**, **b** and **d**, inset) and 250 μm (**d**).

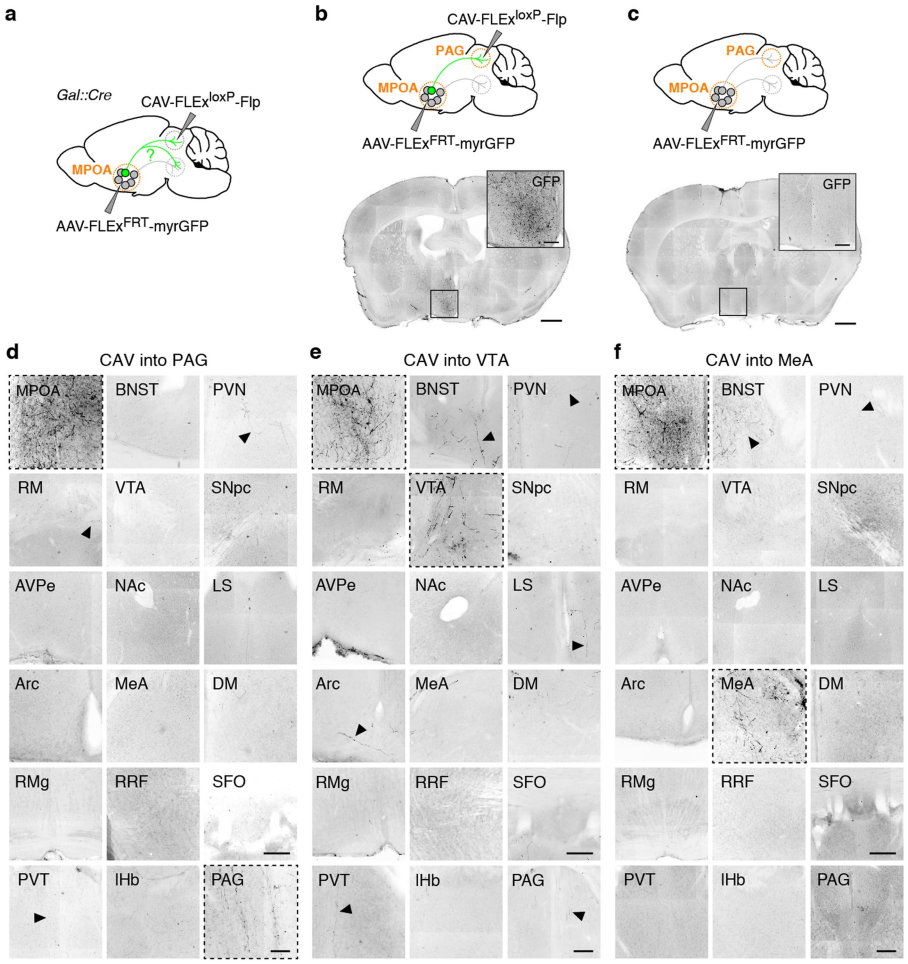

Extended Data Fig. 4 | MPOA^{Gal} projections barely collateralize. **a**, Strategy to detect brain-wide axon collaterals of specific MPOA^{Gal} projections. **b**, Dense labelling of MPOA^{Gal} neurons after injection of retrograde tracer CAV into PAG and reporter AAV into MPOA. **c**, Absence of MPOA^{Gal} labelling in negative control without injection of CAV. **d**–**f**, Only minor axon collaterals are detectable from MPOA^{Gal} neurons projecting to PAG (**d**; $n = 2$ virgin males), VTA (**e**; $n = 3$ virgin males) or MeA (**f**; $n = 2$ virgin males). Note the MPOA to MeA fibre tract in BNST in **f**. Signal was enhanced using anti-GFP immunostaining (Methods). Scale bars, **b**, **c**, 400 μm (**b**, **c**), 100 μm (insets) and 150 μm (**d**–**f**).

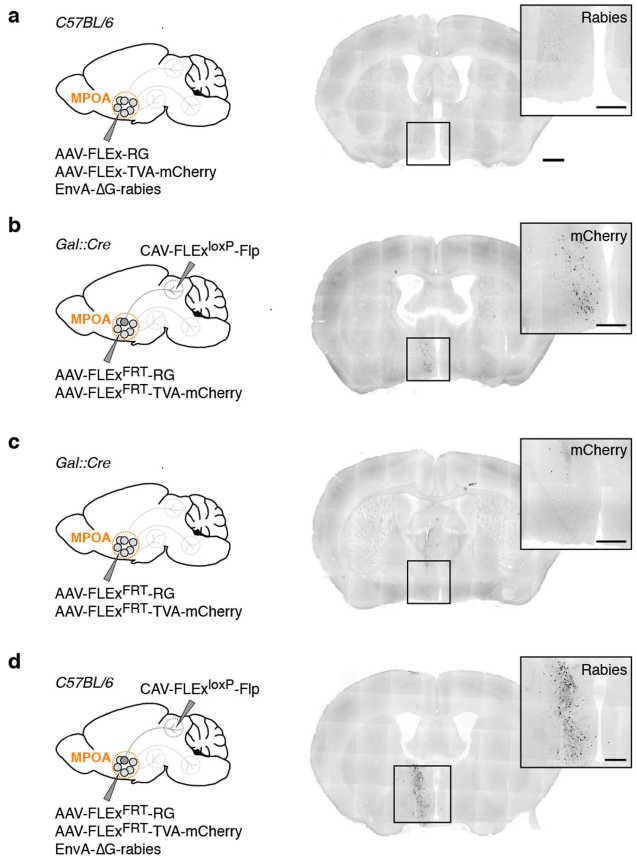

Extended Data Fig. 5 | Negative controls for monosynaptic retrograde tracing. a, Absence of rabies^{+} background labelling in the MPOA of AAV- and rabies-injected C57BL/6 control mice ($n = 2$). **b**, Labelling of MPOA^{Gal} neurons after injection of CAV into PAG and starter AAVs into MPOA of *Gal::cre* mice (261 ± 19 neurons, $n = 4$). **c**, Near-absence of labelling in AAV-only negative control (11 ± 2 neurons, $n = 2$). **d**, Background rabies^{+} neurons were present in the following brain areas of CAV-, AAV- and rabies-injected C57BL/6 control mice ($n = 3$): MPOA, BNST, anterior hypothalamus (AH), PVN and SON. These areas were therefore excluded from analysis (see Fig. 2k, l and Methods). Scale bars, 400 μm (main images) and 150 μm (insets).

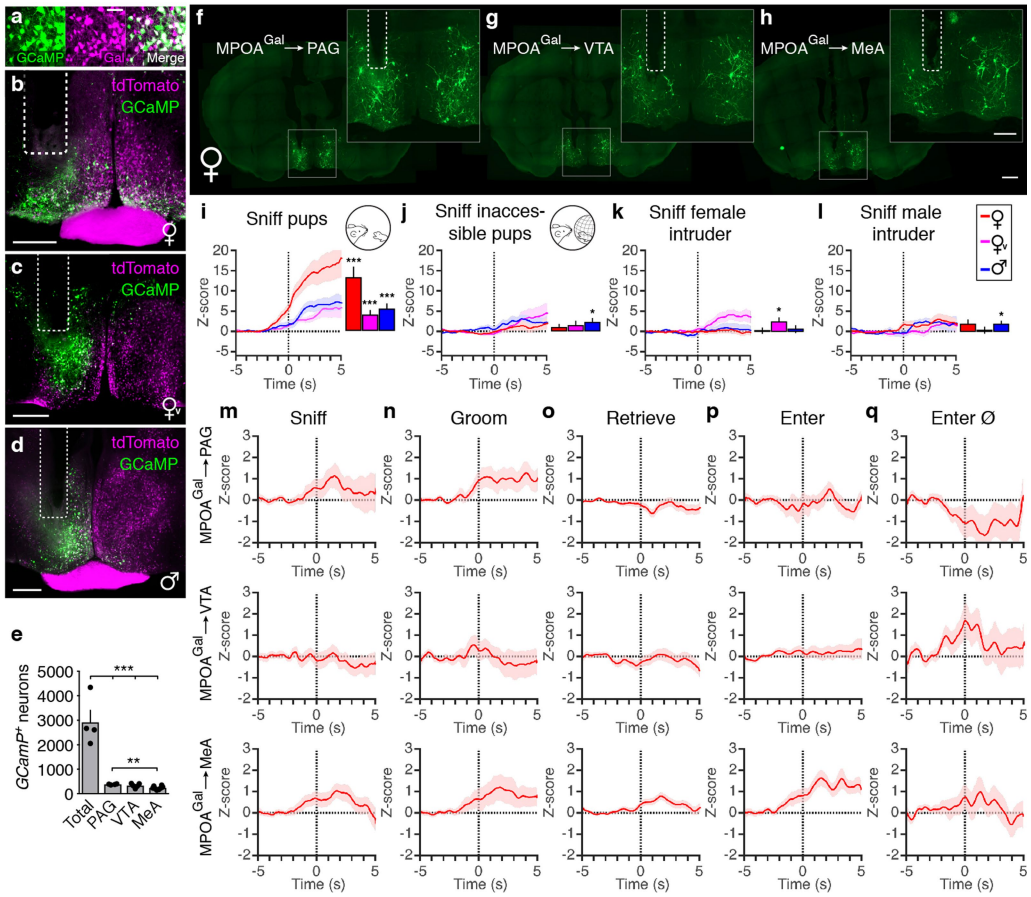

Extended Data Fig. 6 | Histology of photometry recording experiments and tuning of MPOA^{Gal} neurons in other behavioural contexts. **a**, Specific GCaMP6m expression in MPOA^{Gal} neurons (90.9 ± 4.3% overlap, $n = 3$, mothers). **b**–**d**, Implantation sites of optical fibres in the MPOA of *Gal::cre*$^{+/-}$*loxP-Stop-loxP-tdTomato*$^{+/-}$ mother (**b**), virgin female (**c**) and father (**d**). **e**, Quantification of GCaMP^{+} neuron numbers in MPOA after AAV injection ('Total', $n = 4$) and after injection of HSV into individual projections ($n = 5$ each). Data for mothers are shown. Data are mean ± s.e.m. Two-tailed *t*-tests; Total versus PAG, VTA, MeA, $^{***}P < 0.001$, PAG versus MeA, $^{**}P = 0.0033$. **f**–**h**, Expression of GCaMP6m in MPOA^{Gal} neurons after bilateral infection of axon terminals in PAG (**f**), VTA (**g**) or MeA (**h**) with Cre-dependent, GCaMP6m-expressing HSV. Insets show fibre implantation sites. **i**, **j**, Averaged recording traces from MPOA^{Gal} neuron activity during sniffing of accessible pups (**i**) or inaccessible pups enclosed in a wire mesh tea ball (**j**) in mothers ($n = 4$), virgin females ($n = 3$) and fathers ($n = 5$). **k**, **l**, Averaged recording traces from MPOA^{Gal} neuron activity during sniffing of female (**k**) or male (**l**) intruder in mothers ($n = 4$), virgin females ($n = 3$) and fathers ($n = 5$). Two-tailed *t*-tests; **i**, $^{***}P < 0.0001$, $^{***}P < 0.0001$, $^{***}P = 0.0001$ (left to right); **j**, $^{*}P = 0.0380$; **k**, $^{*}P = 0.0219$; **l**, $^{*}P = 0.0272$. **m**–**q**, Averaged recording traces from MPOA^{Gal} neurons projecting to PAG (left, $n = 10$), VTA (middle, $n = 12$) or MeA (right, $n = 8$) during episodes of maternal behaviour. All traces and bar graphs are mean ± s.e.m. Scale bars, 50 μm (**a**), 400 μm (**b**–**d**), 1 mm (**f**–**h**) and 500 μm (**f**–**h**, insets).

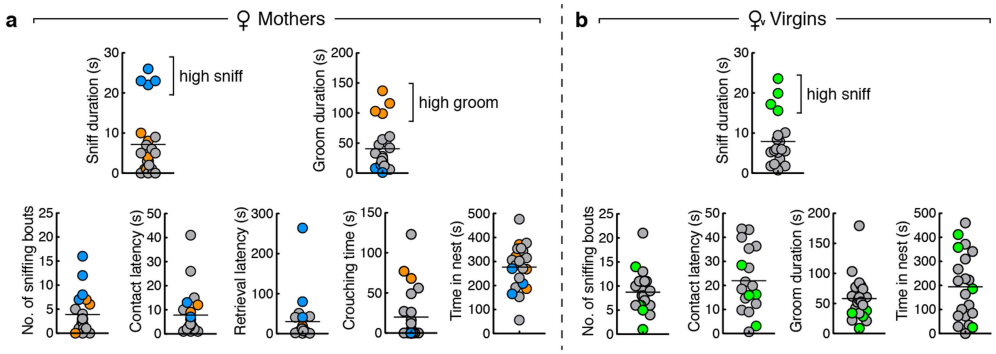

Extended Data Fig. 7 | Distribution of parental behaviours in mothers and virgin females. Distribution of parental behaviours during 10-min pup interaction assays in mothers (**a**; $n = 23$) and virgin females (**b**; $n = 20$). In **a**, individuals exhibiting high pup sniffing are indicated in blue across plots, and individuals exhibiting high pup grooming are indicated in orange. In **b**, individuals exhibiting high pup sniffing are indicated in green. Note that *y* axis ranges are identical between **a** and **b**. Lines depict mean.

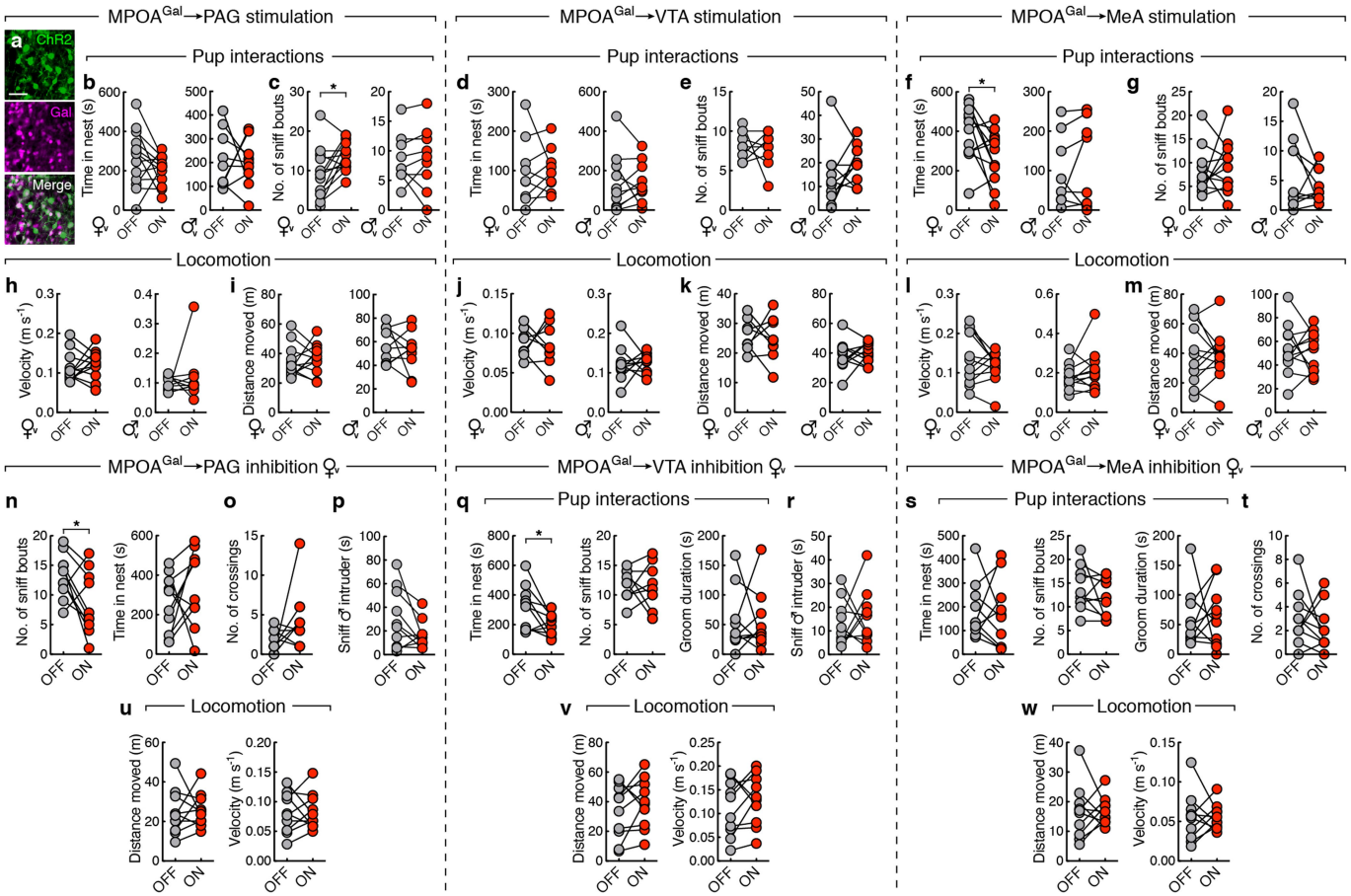

Extended Data Fig. 8 | Behavioural specificity of MPOA^{Gal} projection stimulation. **a**, Channelrhodopsin-2 (ChR2) expression in MPOA^{Gal} neurons (97.7 ± 0.2% overlap, virgin females, $n = 2$). Scale bar, 50 μm. **b**–**g**, Effect of activating PAG (**b**, **c**), VTA (**d**, **e**) or MeA (**f**, **g**) projections on time spent in nest in virgin females and virgin males (**b**, $n = 13$ females and $n = 10$ males; **d**, $n = 9$ females and $n = 10$ males; **f**, $n = 10$ females and $n = 10$ males) and number of pup-directed sniffing bouts (**c**, $n = 13$ females and $n = 10$ males; **e**, $n = 9$ females and $n = 10$ males; **g**, $n = 10$ females and $n = 10$ males). **h**–**m**, Effect of activating PAG (**h**, **i**), VTA (**j**, **k**) or MeA (**l**, **m**) projections on locomotion velocity (**h**, $n = 13$ females and $n = 10$ males; **j**, $n = 8$ females and $n = 10$ males; **l**, $n = 10$ females and $n = 10$ males) and moved distance (**i**, **k**, **m**). **n**, **q**, **s**, Effect of inhibiting PAG (**n**, $n = 10$ females), VTA (**q**, $n = 10$ females) or MeA (**s**, $n = 11$ females) projections on pup interactions. **o**, **t**, Effect of inhibiting PAG (**o**, $n = 10$ females) or MeA (**t**, $n = 11$ females) projections on number of barrier crosses. **p**, **r**, Effect of inhibiting PAG (**p**, $n = 10$ females) or MeA (**r**, $n = 11$ females) projections on chemoinvestigation of a male intruder. **u**–**w**, Effect of inhibiting PAG (**u**), VTA (**v**) or MeA (**w**) projections on locomotion velocity and moved distance ($n = 10$, 10, 11, respectively). Two-tailed paired *t*-tests; **c**, $^*P = 0.0135$; **f**, $^*P = 0.03$; **n**, $^*P = 0.0413$, **q**: $^*P = 0.0264$.

Extended Data Table 1 | List of brain areas and coordinates

Abbreviation	Brain area	Injection coord. (AP / ML / DV)	Stimulation coord. (AP / ML / DV)	Recording coord. (AP / ML / DV)
AH	anterior hypothalamus	–	–	–
AHPM	posteriomedial amygdalohippocampal area	–	–	–
Arc	arcuate nucleus	–	–	–
AVPe	anteroventral periventricular nucleus	0.25 / 0.15 / -5.45	–	–
BMA	basomedial amygdala	–	–	–
BNST	bed nucleus of the stria terminalis	–	–	–
DM	dorsomedial hypothalamus	–	–	–
IL	infralimbic cortex	–	–	–
LC	locus coeruleus	-5.4 / 0.88 / -2.65	–	–
LS	lateral septum	0.4 / 0.3 / -2.5	–	–
MeA	medial amygdala	-1.6 / 2.25 / -4.95	-1.6 / ± 2.25 / -4.5	–
MnPO	median preoptic nucleus	–	–	–
MPOA	medial preoptic area	0 / 0.5 / -5.05	–	0 / 0.5 / -4.9
MS	medial septum	–	–	–
NAc	nucleus accumbens - core	1.0 / 0.7 / -3.8	–	–
NAsh	nucleus accumbens - shell	–	–	–
PAG	(rostral) periaqueductal grey	-3.28 / 0.2 / -2.5	-3.28 / ± 0.2 / -2.2	–
PeFA	perifornical area	-0.6 / 0.3 / -4.2	–	–
PMV	ventral premammillary nucleus	–	–	–
PVN	periventricular hypothalamic nucleus	-0.82 / 0.25 / -4.6	–	–
PVT	periventricular thalamic nucleus	-0.94 / 0 / -2.7	–	–
RM	retromammillary nucleus	–	–	–
RRF	retrorubral field	-4.04 / 1.0 / -3.4	–	–
RMg	raphe magnus nucleus	-5.2 / 0 / -4.55	–	–
SFO	subfornical organ	–	–	–
SNpc	substantia nigra pars compacta	-3.1 / 1.25 / -4.0	–	–
SON	supraoptic nucleus	–	–	–
VMH	ventromedial hypothalamus	-1.5 / 0.4 / -5.7	–	–
VOLT	vascular organ of the lamina terminalis	–	–	–
VTA	ventral tegmental area	-3.0 / 0.6 / -4.2	-3.1 / ±0.5 / -4.1	–

Extended Data Table 2 | Summary of manipulations that affect parenting in MPOA^{Gal} target areas

Brain area	Manipulation	Effect	Reference
PAG	Lesion	Facilitates maternal responses	45
	$GABA_A$ receptor antagonist	Decreases maternal aggression, increases pup licking / grooming	19
MeA	Lesion	Accelerates onset of maternal behaviour	46-48
PVN	Lesion	Disrupts onset of maternal behaviour	49 (but see 50)
LS	$GABA_A$ receptor antagonist	Decreases maternal aggression	51
	Corticotropin releasing factor	Decreases maternal aggression	52
LC	Disruption of 5-HT production	Disrupts maternal behaviour (mice)	53
AVPe	Ablation of TH^+ neurons	Impairs maternal behaviour (mice)	11
	Optogenetic stimulation of TH^+ neurons	Enhances maternal behaviour (mice)	
VTA	Lesion	Impairs pup retrieval	2,53
	Inactivation	Impairs pup-paired conditioned place preference	22
NAc	Lesion	Impairs pup retrieval	54,55
	DA receptor antagonist	Inhibits retrieval and licking; enhances nursing	56,57
SNpc	Lesion	Disrupts maternal behaviour	58
VMH	Lesion	Accelerates onset of maternal behaviour	59
BNST	Lesion (ventral BNST)	Disrupts maternal behaviour	60
	Estrogen injection	Facilitates maternal responses	61
	Prolactin injection	Facilitates maternal responses	62
RRF	n/a	RRF-projecting MPOA neurons activated during maternal behaviour	63
PVT	n/a	Activated during maternal behaviour	64

From those brain areas targeted by MPOA^{Gal} projections (Fig. 2c), manipulation of the following areas has been shown to affect maternal behaviour in rats (or mice where indicated)[45–64]. For a more comprehensive review see Kohl et al.[10].

nature research

Corresponding author(s): Catherine Dulac, PhD

☐ Initial submission ☐ Revised version ☒ Final submission

Life Sciences Reporting Summary

Nature Research wishes to improve the reproducibility of the work that we publish. This form is intended for publication with all accepted life science papers and provides structure for consistency and transparency in reporting. Every life science submission will use this form; some list items might not apply to an individual manuscript, but all fields must be completed for clarity.

For further information on the points included in this form, see Reporting Life Sciences Research. For further information on Nature Research policies, including our data availability policy, see Authors & Referees and the Editorial Policy Checklist.

Experimental design

1. Sample size

Describe how sample size was determined.

No statistical methods were used to predetermine sample size, but sample sizes are consistent with those generally employed in the field.

2. Data exclusions

Describe any data exclusions.

In fibre photometry and optogenetics experiments, mice with no expression of the virus, or fibre tip placement outside of the target structure were excluded from the analysis.

3. Replication

Describe whether the experimental findings were reliably reproduced.

All attempts at replication were successful.

4. Randomization

Describe how samples/organisms/participants were allocated into experimental groups.

Animals were randomly assigned numbers and tested blind for the experimental condition.

5. Blinding

Describe whether the investigators were blinded to group allocation during data collection and/or analysis.

All behavioural experiments were scored by an individual blind to the genotype and experimental design.

Note: all studies involving animals and/or human research participants must disclose whether blinding and randomization were used.

6. Statistical parameters

For all figures and tables that use statistical methods, confirm that the following items are present in relevant figure legends (or in the Methods section if additional space is needed).

n/a	Confirmed
☐	☒ The exact sample size (*n*) for each experimental group/condition, given as a discrete number and unit of measurement (animals, litters, cultures, etc.)
☐	☒ A description of how samples were collected, noting whether measurements were taken from distinct samples or whether the same sample was measured repeatedly
☐	☒ A statement indicating how many times each experiment was replicated
☐	☒ The statistical test(s) used and whether they are one- or two-sided (note: only common tests should be described solely by name; more complex techniques should be described in the Methods section)
☐	☒ A description of any assumptions or corrections, such as an adjustment for multiple comparisons
☐	☒ The test results (e.g. *P* values) given as exact values whenever possible and with confidence intervals noted
☐	☒ A clear description of statistics including central tendency (e.g. median, mean) and variation (e.g. standard deviation, interquartile range)
☐	☒ Clearly defined error bars

See the web collection on statistics for biologists for further resources and guidance.

Software

Policy information about availability of computer code

7. Software

Describe the software used to analyze the data in this study.	Statistical analyses were performed in Graphpad Prism 7.0c or using custom Matlab or R routines. Ethovision XT 8 software (Noldus) was used for animal tracking. Observer 5.0 (Noldus) was used for behavioural scoring. Image processing was performed using custom routines for the Fiji distribution of ImageJ (Version 2.0.0-rc-43); Adobe Illustrator CC (2014) for assembling figures; Adobe After Effects CC for video rendering.

For manuscripts utilizing custom algorithms or software that are central to the paper but not yet described in the published literature, software must be made available to editors and reviewers upon request. We strongly encourage code deposition in a community repository (e.g. GitHub). *Nature Methods* guidance for providing algorithms and software for publication provides further information on this topic.

Materials and reagents

Policy information about availability of materials

8. Materials availability

Indicate whether there are restrictions on availability of unique materials or if these materials are only available for distribution by a for-profit company.	All unique materials are readily available from the authors.

9. Antibodies

Describe the antibodies used and how they were validated for use in the system under study (i.e. assay and species).	All antibodies used were commercial and validated (see manufacturer's website). Primary antibodies: goat anti-c-Fos (Santa Cruz, sc-52) 1:500, chicken anti-GFP (Abcam, ab13970) 1:1,000, rabbit anti-AVP (Immunostar, 20069) 1:6,000, rabbit anti-OXT (Immunostar, 20068) 1:6,000. Secondary antibodies (all from Thermo Fisher): Alexa-568 anti-goat (A-11057) 1:1,500, Alexa-555 anti-goat (A-21432) 1:1,500, and Alexa-647 anti-goat (A-21447) 1:1,500.

10. Eukaryotic cell lines

a. State the source of each eukaryotic cell line used.	No eukaryotic cell lines were used.
b. Describe the method of cell line authentication used.	No eukaryotic cell lines were used.
c. Report whether the cell lines were tested for mycoplasma contamination.	No eukaryotic cell lines were used.
d. If any of the cell lines used are listed in the database of commonly misidentified cell lines maintained by ICLAC, provide a scientific rationale for their use.	No eukaryotic cell lines were used.

Animals and human research participants

Policy information about studies involving animals; when reporting animal research, follow the ARRIVE guidelines

11. Description of research animals

Provide details on animals and/or animal-derived materials used in the study.	Mice of the following strains were used, at 8-12 weeks of age: Tg(Gal-cre)KI87Gsat/Mmucd (Gal::Cre, Mutant Mouse Regional Resource Center), Gt(ROSA)26Sortm9(CAGtdTomato)Hze, C57BL/6J (JAX), Oxt-ires-Cre, Vgat-ires-Cre and TH-ires-Cre (all from Jackson Laboratories); Vglut2-ires-Cre (provided by B. Lowell, Harvard Medical School); Avp-ires-Cre (described in Bendesky et al. 2017, PMID: 28424518). Both males and females were separately tested in most experiments as indicated in the manuscript.

Policy information about studies involving human research participants

12. Description of human research participants

Describe the covariate-relevant population characteristics of the human research participants.	The study did not involve human research participants.